GoNEXUS

Tools and solutions for governing the nexus

Upscaling Feedbacks

Deliverable D4.3 – WP4
July 2024

GoNEXUS has received funding from the European Union's Horizon 2020 research and innovation programme under grant agreement number 101003722.

www.gonexus.eu

Version 0.3
July, 2024

Deliverable D4.3: Upscaling Feedbacks
Lead by POLIMI
Matteo Giuliani, Teresa Bonserio, Arianna Leoni, Andrea Castelletti (POLIMI); Hector Macian-Sorribes, Manuel Pulido-Velazquez (UPV);

Dissemination level of document
Public

Abstract
This document synthetizes the main findings of WP4 Task T4.6 (Feedbacks to the global scale) which aim to identify gaps between global and local Water-Energy-Food-Ecosystem models identified when navigating the trade-off between targeting realism at the local scale and representing global socio-economic and climatic teleconnections. The report covers different types of feedback involving selected GONEXUS case studies and diverse spatial scales.

GoNEXUS has received funding from the European Union's Horizon 2020 research and innovation programme under grant agreement number 101003722.

Version History

Version	Date	Authors	Description
V0.1	10/05/2024	Matteo Giuliani, Andrea Castelletti (POLIMI)	Proposed structure of the report
V0.2	18/07/2024	T. Bonserio, A. Leoni, A. Castelletti, M. Giuliani, H. Macian-Sorribes, M. Pulido-Velazquez	POLIMI-UPV contributions added
V0.3	31/07/2024	T. Bonserio, A. Leoni, A. Castelletti, M. Giuliani, H. Macian-Sorribes, M. Pulido-Velazquez	Review

Table of contents

1 Introduction

This document synthetizes the main findings of Task T4.6 (Feedbacks to the global scale) which aim to identify gaps between global and local Water-Energy-Food-Ecosystem models identified when navigating the trade-off between targeting realism at the local scale and representing global socio-economic and climatic teleconnections. The report covers different types of feedback involving selected GONEXUS case studies and diverse spatial scales.
Specifically, we discuss in detail four feedback:

- the integration of reservoir operating rules in global hydrologic models (Chapter 2);
- the estimation of hydropower capacity factors in energy models conditioned upon water availability (Chapter 3);
- the impacts of political instability on power trade vulnerability (Chapter 4);
- the refinement of continental multi-decadal energy planning to regional, hourly power dispatch dynamics (Chapter 5).

Besides, in Chapter 6 we illustrate the discrepancies between an estimation of local water scarcity functions for the Jucar River Basin with respect to those used by CAPRI model at the continental scale. Finally, we point the reader to Deliverable D3.2 for the analysis of the uptake of European agricultural policies.
In each chapter, we explored the different feedback identified and discuss their implications for the global/continental models used by policy makers in prioritizing mitigation and adaptation policies.
As shown by the GoNEXUS interactions depicted in Figure 1, the findings of this deliverable combined with those of Task 3.3, will support the model toolbox in advancing WEFE models for supporting the generation of evidence in WP5.

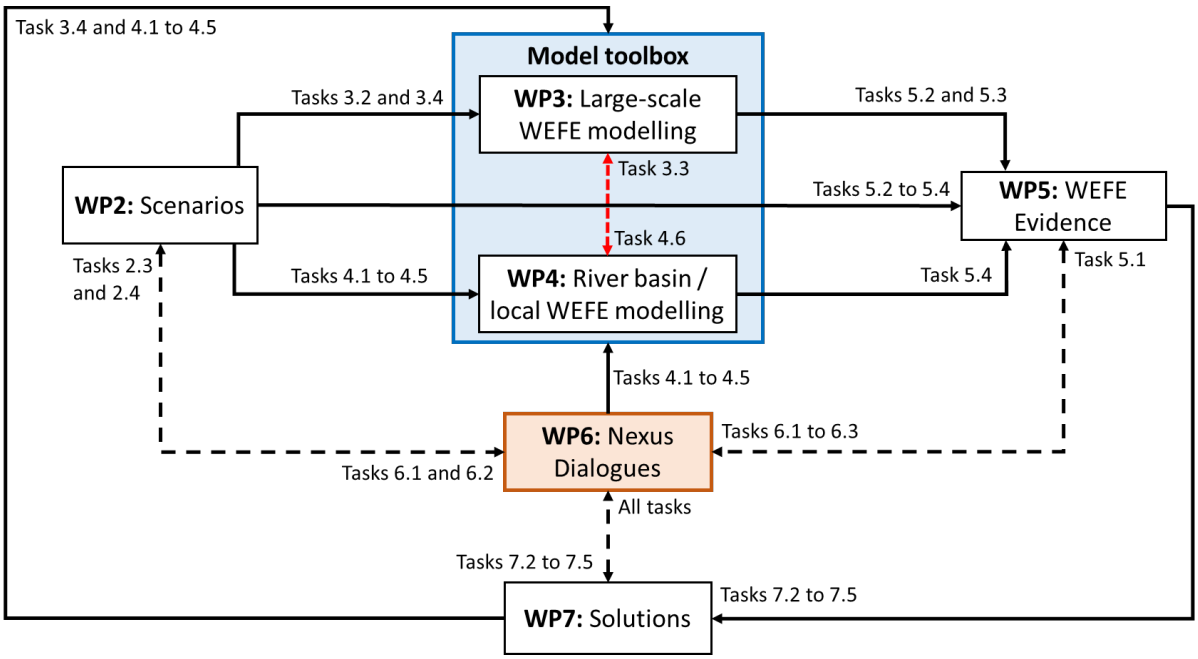

Figure 1: GoNEXUS interconnections.

2 Integrating reservoir operating rules in global hydrologic models

Including reservoir regulation in large-scale hydrologic models is one of the main challenges in the field nowadays, in particular when addressing extreme events such as droughts (Wada et al., 2017) Although many alternatives exist to represent reservoir operating rules in large-scale hydrologic models, including purpose-depending configurations (Van Beek et al., 2011), the representation of multi-reservoir operation is still a challenge.

In this context, artificial intelligence approaches emerge as an efficient opportunity to address this challenge, given its adaptative formulation. This feedback describes the development of a mathematical representation of reservoir operating rules for multipurpose multi-reservoir systems.

2.1 Methodology

Among the available artificial intelligence (AI) methodologies available, fuzzy logic was chosen to develop reservoir operating rules. It has been applied to derive both historical (Bai and Tamjis, 1970; Macian-Sorribes and Pulido-Velazquez, 2017; Shrestha et al., 1996) and optimal (Kumar et al., 2013; Panigrahi and Mujumdar, 2000; Russell and Campbell, 1996) operating rules. Fuzzy logic maps input variables to outputs using sets of fuzzy logical rules expressed through IF-THEN statements (Mamdani, 1974):

IF x is A and y is B, THEN output is C

Compared to Boolean logic, fuzzy logic is supported by linguistic descriptors attached to fuzzy numbers, such as "low", "moderate" or "high". The previous rule can be re-written in a fuzzy logic format by changing A, B and C to those linguistic descriptors:

IF x is LOW and y is HIGH, THEN output is MODERATE

Furthermore, a fuzzy logical rule is not subject to the Boolean to be or not to be approach, in which a rule is either followed (logical value 1) or not followed (logical value 0). A fuzzy logic rule, on the contrary, could be either fully followed (logical value 1), partially followed (logical values between 0 and 1) or not followed (logical value 0). This feature is closer to real-world applications and turns fuzzy logic into a flexible approach (Ekel et al., 2010). Moreover, the link between fuzzy numbers and linguistic descriptors facilitates the uptake of expert knowledge in fuzzy rules.

A fuzzy rule-based (FRB) system, also known as fuzzy inference system (FIS) or fuzzy logic system, is defined by a set of fuzzy rules, the fuzzy numbers that quantify their premises and consequences, and mathematical operators. In order to create and use a fuzzy rule-based system, several stages are needed. The following description of both processes is based on Macian-Sorribes et al (2020) Macian-Sorribes and Pulido-Velazquez (2017).

2.1.1 Fuzzy rule-based system building

Although the methodology is described in general terms, it contains some adaptations made by the literature in order to adapt it to the specific features of water resources management; and thus it may differ from fuzzy logic descriptions for other science fields. The process required to build a FRB system is shown in Figure 2.

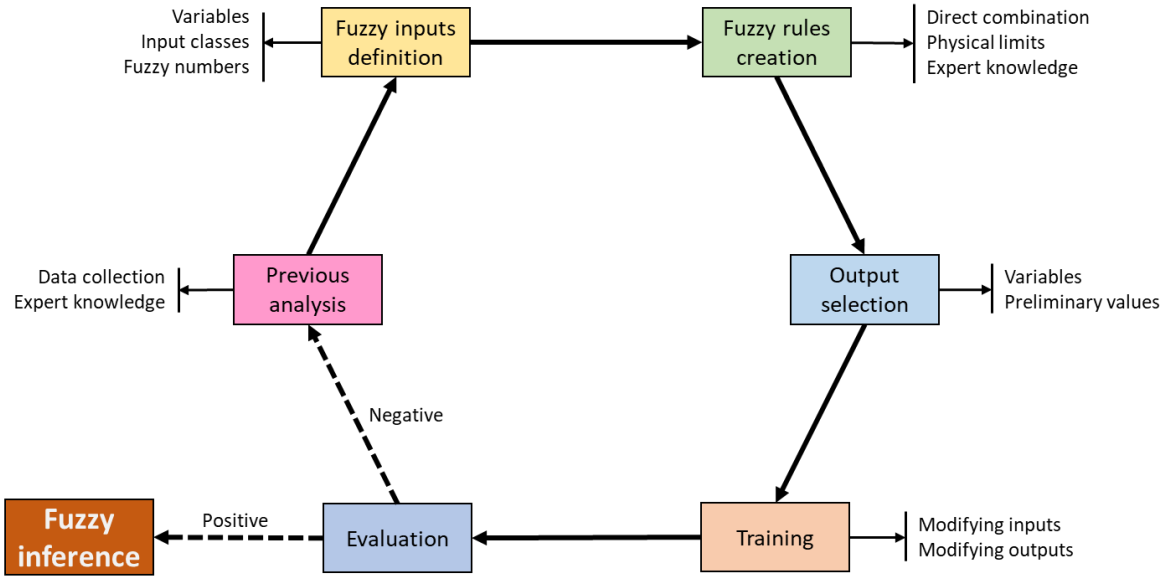

Figure 2. FRB system building stages (modified from Macian-Sorribes et al, 2020)

2.1.1.1 Previous analysis

The previous analysis is a common stage in any algorithmic application, consisting in collecting the required data and information to develop the FRB system in a proper way to achieve its goals. In the case of fuzzy logic, this stage also includes setting the blueprint of expert knowledge acquisition if any.

2.1.1.2 Fuzzy inputs definition

The choice of fuzzy inputs has three substages: variable choice, division of each input variable in classes and attaching a fuzzy number to each class. Defining the input variables depend on the goal of the FRB, the available information, the temporal scale at which the FRB system will work and the system features. In water resources management, typical input variables include initial storages or levels, inflows, downstream demands and the time of the year (e.g. season, month, week).

Once variables are set, each one should be divided by classes typically attached to linguistic descriptors (e.g. one variable divided in three classes could be characterized by the linguistic descriptors "low", "medium" and "high"). The number of classes is conditioned by the goal of the FRB system and the available information: a large number of classes implies an increase in the system's ability to reproduce the desired behaviour but in turn it increases the training complexity. If a very large number of classes is found, linguistic descriptors might be skipped,

since the differences between them would be less evident. It might be taken into account that these linguistic descriptors are key in case of using expert knowledge.

Once the number of classes per variable is decided, it is required to attach one fuzzy number to each class (and to the linguistic descriptor if used). The definition of fuzzy numbers can be done based on several criteria such as expert knowledge, equal spacing or based on the historical records available.

2.1.1.3 Fuzzy rules creation

Fuzzy rules are made by combining the fuzzy inputs previously created based on their classes. The most straightforward way is to directly combine each class with all the classes of the remaining input variables, and thus the total number of rules would be the product of the classes of all inputs (e.g. a FRB system with 2 inputs of 5 classes each would have 5·5 = 25 rules; and one with 3 inputs of 5, 3 and 3 classes would have 5·3·3 = 45 rules).

However, a most precise fuzzy rule set could be defined in situations in which physical limits apply (e.g. in case of a fuzzy logic system with coordinates and rainfall is inputs, a fuzzy rule depicting the combination between very high rainfall and coordinates of desertic areas would not ring any bell) or in case that expert knowledge labels some of them as infeasible or improbable. An example of fuzzy rules with one input with two classes and the other with three classes is shown in Table 1.

Table 1. Example of fuzzy rules

Fuzzy rule	Input 1	Input 2
1	LOW	LOW
2	LOW	MEDIUM
3	LOW	HIGH
4	HIGH	LOW
5	HIGH	MEDIUM
6	HIGH	HIGH

Besides the fuzzy rules, it is required to define the mathematical operator that will be used to determine in which degree each fuzzy rule will be followed, based on how its premises are followed. Typical operators are the logical operators ("AND", minimum among degrees of fulfilment; "OR", maximum among degrees of fulfilment), the product of all the degrees of fulfilment or the squared product of all of the them. The degree of fulfilment is the logical value that each input has compared to the fuzzy numbers used to characterize the inputs of each rule, ranging between 0 and 1. More details can be found in the next 2.1.2 section below.

2.1.1.4 Output selection

Similar to input definition, output selection implies choosing the output variables based on the goals pursued and the information available, as well as quantifying them. Typical outputs of FRB systems for water resource operation involve target releases (global or per demand) or target storages or levels.

In contrast to the previous stages, outputs can either be fuzzy or non-fuzzy numbers. Fuzzy outputs are used by a Mamdani FRB, while non-fuzzy ones are characteristic of a Sugeno FRB. In the latter, the outputs are the coefficients of a polynomial equation whose order defines the order of the Sugeno FRB (e.g. a Sugeno FRB system of order 1 would employ linear equations, meaning that each rule would have two output values per output variable: the independent term and the slope). In the following, non-fuzzy input configurations (and thus a Sugeno FRB) will be considered. Together with the definition of output variables, preliminary values need to be attached to them. In a Sugeno FRB, each fuzzy rule should be given one preliminary output set value, which might change during the training process.

2.1.1.5 Training

The training stage consists in adjusting the response of the FRB system to the desired behaviour, either historical observations, expert knowledge information or algorithm's results that should be mimicked. One FRB system can be trained by modifying the outputs or jointly changing inputs and outputs. Although the latter option would theoretically achieve a better performance compared to the former, in makes more difficult the training process itself and, in case of inputs defined by expert knowledge, would imply the loss of this knowledge. On the other hand, training the FRB system modifying exclusively the outputs is easier and it is the option mostly used in the literature on fuzzy logic applied to reservoir management.

2.1.1.6 Evaluation

The evaluation is developed by measuring the performance of the FRB system using input data not employed for training. In case it is not adequate, the building process needs to be restarted. In case it is positive, the usage of the FRB system is enabled.

2.1.2 Fuzzy rule-based system use (fuzzy inference)

The use of a trained and evaluated FRB system is also known as fuzzy inference and consists in mapping inputs to outputs. It follows the stages depicted in Figure 3.

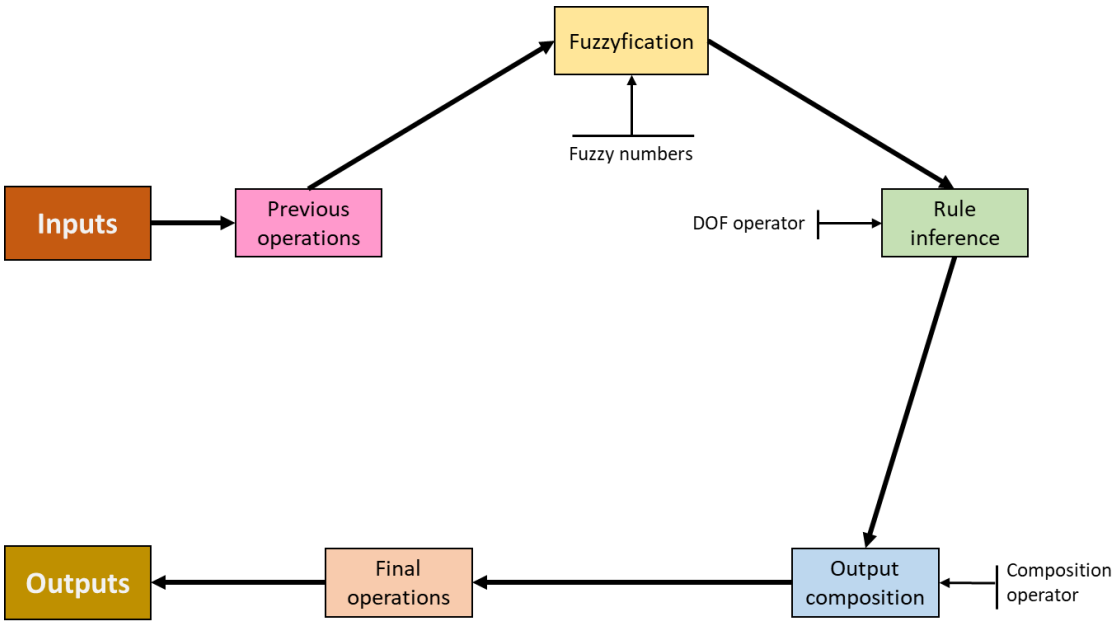

Figure 3. Fuzzy inference stages (modified from Macian-Sorribes et al, 2020).

2.1.2.1 Previous operations

This step is applicable in case that the input variables need some pre-processing before introducing them into the FRB system, such as change of spatial or temporal scale and change of units.

2.1.2.2 Fuzzyfication

The fuzzification calculates how the input values (which are non-fuzzy) match the fuzzy numbers attached to each input class and, if used, to the linguistic descriptors. This calculation is performed by comparing, for each input, its actual non-fuzzy value with all the fuzzy numbers used to characterize this variable, in order to determine the degree to which the input value corresponds to them (also known as membership degree or membership value).

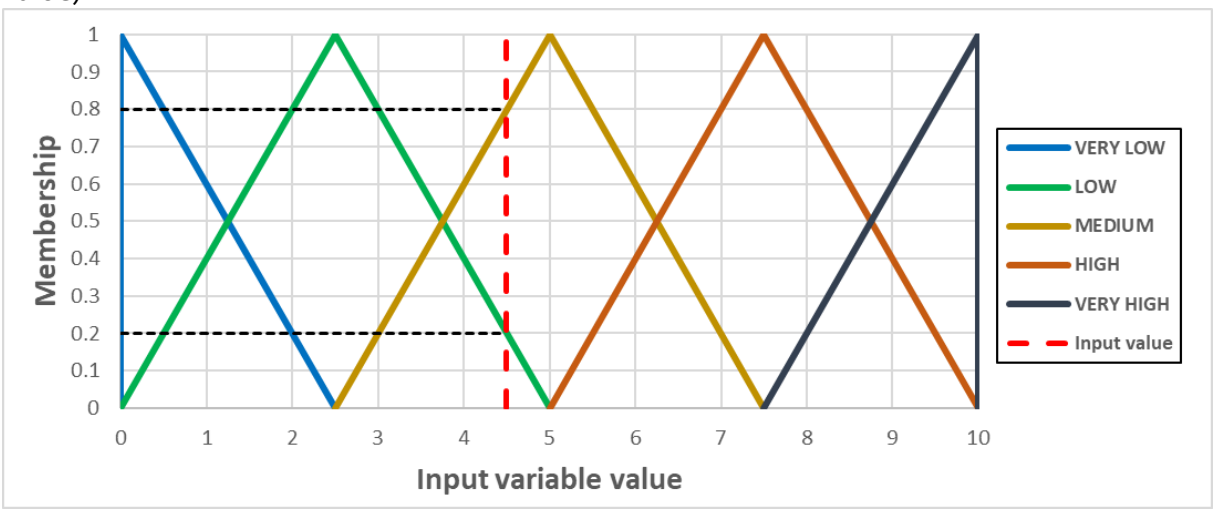

Figure 4 shows an example of fuzzification, in which a value of 4.5 in a given fuzzy number would result into a membership value of 0.2 in the "low" class, 0.8 in the "medium" class and 0 in the rest of classes.

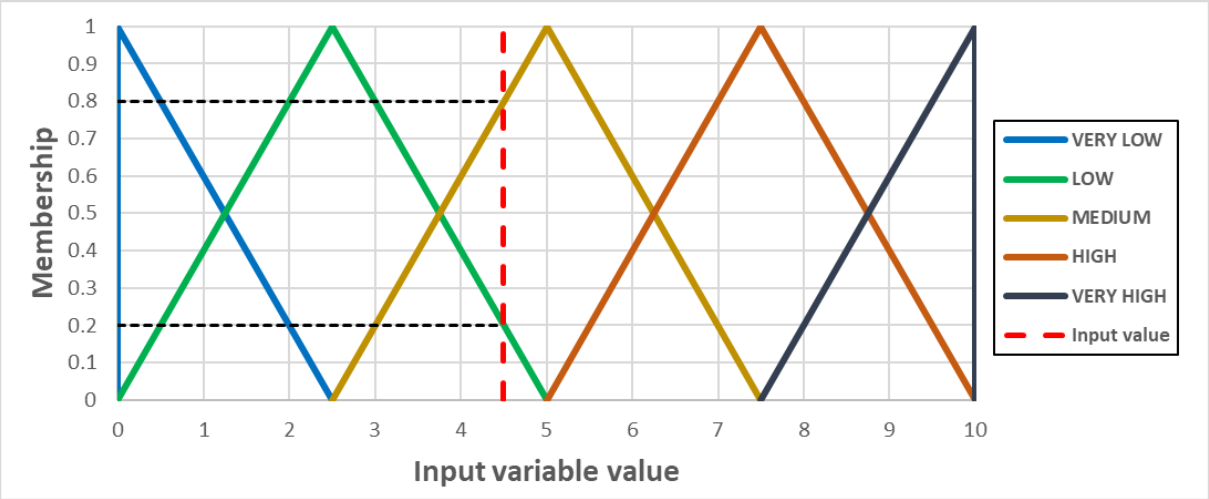

Figure 4. Fuzzyfication.

2.1.2.3 Rule inference

The rule inference process uses the membership degrees obtained in the fuzzification stage for all the inputs to determine the degree of fulfilment of each fuzzy rule. It consists in applying the operator defined in the FRB building process to each fuzzy rule. For example, in case of using the product operator, the degree of fulfilment of a fuzzy rule such as "*if input 1 is LOW and input 2 is LOW*" would be calculated by multiplying the membership degrees of the inputs corresponding to the "LOW" fuzzy number.

2.1.2.4 Output composition

This stage computes the output of the FRB system based on the outputs of all the fuzzy rules and their degrees of fulfilment. In case of a Sugeno FEB system, this process is performed by computing, for each output variable, the weighted average over all the fuzzy rules, in which the weights are the degrees of fulfilment of each rule.

2.1.2.5 Final operations

The final operations are required when refining the output values is necessary (e.g. adjusting releases to the physical constraints of the outlets or to avoid negative values in one or more reservoirs.

2.1.3 Experimental setup

The schematic of the FRB system used to represent the operating rules of the Jucar river system is shown in Figure 5. The FRB system was coded in the Python programming language. A Sugeno FRB system of order 1 was chosen. It has four inputs (the current storages in the Alarcon, Contreras and Tous reservoirs, which are the main Jucar river reservoirs and the ones introduced in PCR-GLOBWB2; plus the month of the year) and three outputs (the

releases from Alarcon, Contreras and Tous). The FRB system is defined to work at the daily scale, and thus the release is adjusted on a daily basis. In spite of this temporal scale, it has been considered that using the month of the year as input instead of the actual day or week is appropriate given that operation decisions tend to be stable over the same month. The use of inflows as input has been discarded given that, at the daily scale, the size of the reservoirs is two or even three orders of magnitude above the incoming streamflows, which implies that do not play a role in defining operating decisions.

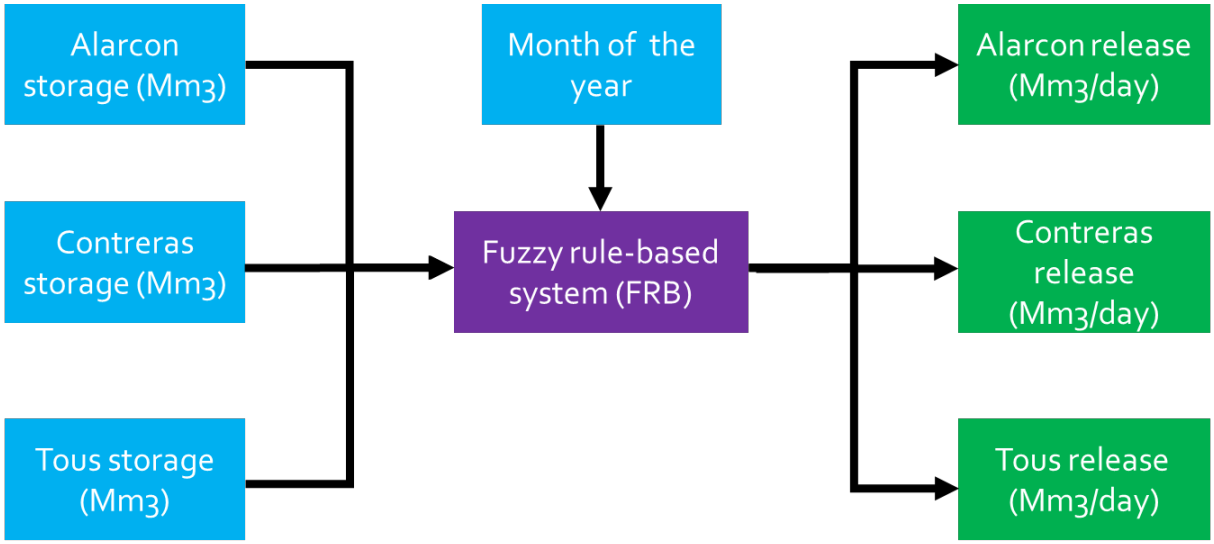

Figure 5. Schematic of the FRB system to reproduce the Jucar river operating rules.

Concerning inputs, the month of the year was defined as a non-fuzzy input divided in classes, representing each one a month of the year. This accommodation of non-fuzzy inputs in an FRB system, in practical terms, means that the FRB system works separately for each month, and thus it is equivalent as 12 FRB systems defined each one for a particular month. This setup is efficient because it enables a more precise definition of inputs and facilitates the training of the FRB system since the rules corresponding to each month can be trained separately from the rest. The remaining inputs were characterized by using three classes ("LOW", "MEDIUM" and "HIGH") and attaching to each one a fuzzy number depending on the monthly minimum, median and maximum values (Figure 6). For each month, the fuzzy number representing a "LOW" storage ranges between an empty reservoir (0) and the median value of the data records for the given month, with a modal value (value in which the membership of the fuzzy number is equal to 1) defined as the minimum value recorded for the given month. The fuzzy number of "MEDIUM" ranges between the minimum and the maximum values for the given month, with a modal value equal to the median. The "HIGH" fuzzy number ranges between the mediant value per month and the capacity of the reservoir, with a modal value equal to the maximum record for the same month. This division guarantees that all rules will be triggered during the training period, and also provides a level of overlap between fuzzy numbers within the recommendations of the literature, in which overlapping of fuzzy numbers is desirable. The operator to define the degree of fulfilment of each rule has been defined as the product among all input variables.

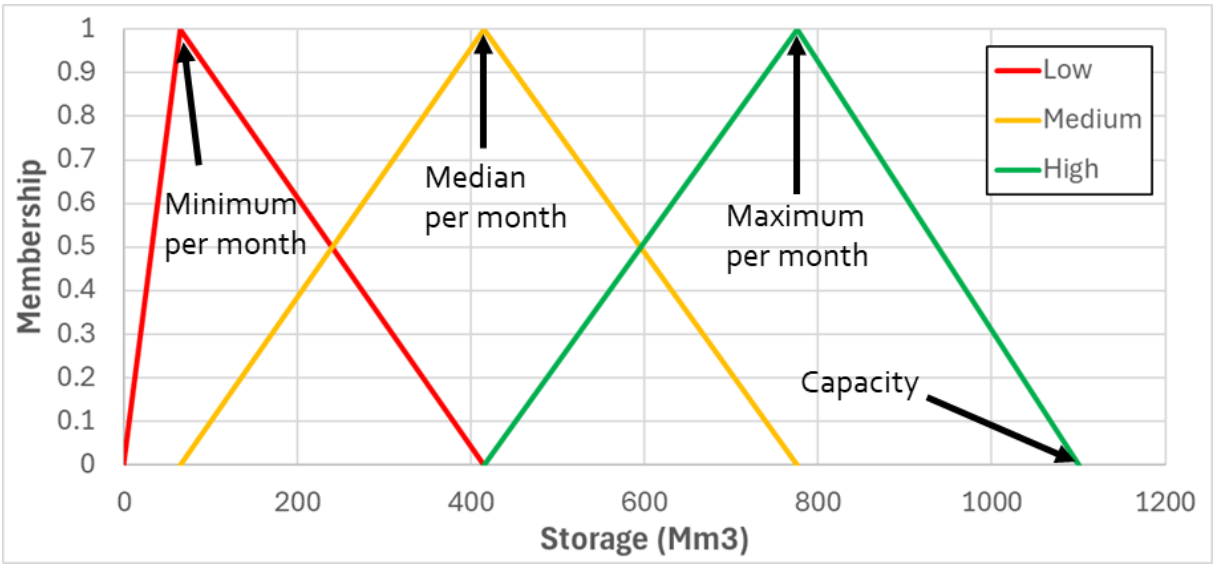

Figure 6. Fuzzy input characterization of storages adopted.

The available data records on storages, inflows and releases from the three reservoirs used to train and validate the FRB system ranges between October 2005 and September 2019. Instead of separating the training and the evaluation period depending on the year, it has been preferred to do it based on the days of the month. Consequently, the data records corresponding to the 1st, 8th, 15th and 22nd days of each month were used to train the FRB system, while the rest of the days were employed in the evaluation process. The preliminary values given to the independent terms for each rule were the average of the historical releases for the month that corresponds to the rule, while the null preliminary values were adopted for the slope terms. The training was performed using the Pyomo Python library and the IPOPT algorithm (Interior Point OPTimizer, https://www.coin-or.org/)

2.2 Numerical Results

Given that performing a training coupling the FRB system with PCR-GLOBWB2 would be infeasible due to the computational burden required, an offline training has been performed by using historical observations as input variables instead of PCR-GLOBWB2 results. This process is faster, but it implies that the results shown are an upper bound of the ones that would be achieved once implemented in PCR-GLOBWB2. Figure 7 and Table 2 summarize the performance achieved by the FRB system in reproducing the observed releases, including both training and evaluation data.

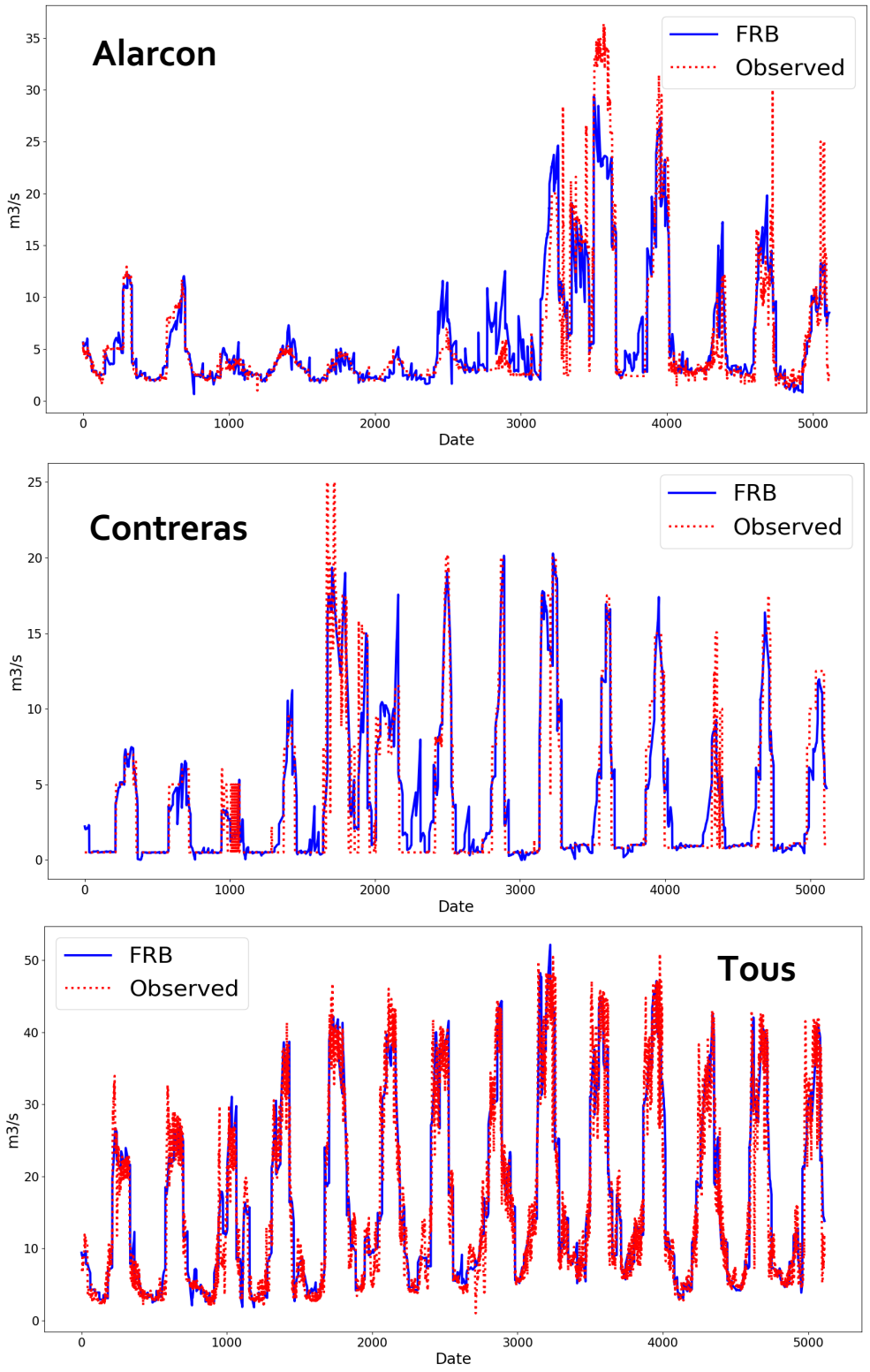

Figure 7. Performance of FRB system for Jucar river reservoir operation.

In all cases the metrics achieved show a good performance level, with similar values of the Nash-Sutcliffe efficiency index (NSE) and similar Root Mean Squared Error in absolute terms,

although the normalized RMSE yields lower values for Tous because of its higher releases compared to Alarcon and Contreras. Furthermore, the plots show an adequate reproduction of the historical values, in particular for the Tous reservoir, which is quite relevant since it is the one placed downstream, so its releases directly condition the water availability in the lower Jucar, which concentrates the majority of the surface water uses. In Alarcon and Contreras the FRB system shows some periods in which it overestimates the required releases, followed in the case of Alarcon by a period in which the opposite happens.

Table 2. Performance metrics of the FRB system for Jucar river reservoir operation.

Reservoir	NSE	NRMSE
Alarcon	0.80	0.50
Contreras	0.84	0.54
Tous	0.88	0.28

In conclusion, the FRB system developed for the Jucar river system shows a good performance level with a relatively simple experimental setup (27 rules per month), reinforcing the potential of fuzzy logic to derive adequate operating rules for multi-reservoir systems with complex operation patterns such as the Jucar.

3 Advancing the estimation of hydropower capacity factors in energy models

In state-of-the-art energy systems modelling, reservoir hydropower is represented as any other thermal power plant: energy production is constrained by the plant's installed capacity and a capacity factor calibrated on the energy produced in previous years (Stevanato et al., 2021). Yet, hydropower generation is largely dependent upon hydroclimatic variability, which may either curtail production during intense drought events that reduce water availability, leading to biased optimal power dispatch strategies (Carlino et al., 2021).
In this chapter, we aim to advance the representation of hydropower generation in energy systems models by conditioning the capacity factors of this technology upon the water available at the power plant location as estimated by hydrological models. The proposed approach is demonstrated using the OSeMOSYS-TEMBA model of the African energy system (Pappis et al., 2019) estimating the capacity factors of the 633 hydropower plants included in the African Hydropower Atlas (Sterl et al., 2022). Our estimate of the capacity factors are based on the SWAT+ hydrological model that is used to simulate the water availability both under the historical time period (1980-2016) and under different future ISIMIP2b scenarios over the period 2020-2050 (Carlino et al., 2023).

3.1 Methodology

Hydropower plants are categorized into three main types: (i) run-of-river, (ii) reservoir, and (iii) cascade configurations. Each type has distinct operational characteristics and outflow profiles, which are subsequently converted to the corresponding capacity factors. This process is run for three different hydrologic conditions, namely normal, dry and wet conditions. Normal capacity factors are derived as the monthly median, while wet and dry are obtained by multiplying the monthly median profiles by the ratio of 5th and 95th percentile of annual generation to multi-annual average generation.

3.1.1 Run-of-River Hydropower Plants

For run-of-river plants, the outflow profile is equivalent to the inflow profile. Power generation is modeled as a linear function of this outflow, capped at the design discharge to reflect full capacity operation during multiple months, not just the wettest. Seasonal capacity factors are calculated as follows:

$$\langle CF_{hydro} \rangle_m^{n,d,w} = min\left(\frac{\langle Q(t) \rangle_m^{n,d,w}}{Q_{design}}, 1 \right)$$

Where $\langle CF_{hydro} \rangle_m^{n,d,w}$ is the capacity factor for month *m* in normal (*n*), very dry (*d*), or very wet (*w*) years, $\langle Q(t) \rangle_m^{n,d,w}$ is the average turbined outflow in that month, and Q_{design} is the design discharge.

If Q_{design} is unknown, it is estimated using the multiannual mean river discharge Q_{mean} and an assumed multiannual average capacity factor $\overline{CF}$, typically 50%:

$$\langle CF_{hydro} \rangle_m^{n,d,w} = min\left(\frac{\langle Q(t) \rangle_m^{n,d,w}}{Q_{mean}} \times \overline{CF}, 1 \right)$$

When neither Q_{design} nor Q_{mean} are available, the design discharge is assumed to be 50% of the maximum monthly flow in a normal year:

$$\langle CF_{hydro} \rangle_m^{n,d,w} = min\left(\frac{\langle q(t) \rangle_m^{n,d,w}}{0.5 \times q_{max,n}} \times \overline{CF}, 1 \right)$$

Where *q(t)* is the flow time series before bias-correction, and $q_{max,n}$ is the maximum monthly flow in a normal year. Calculations are performed separately for normal, dry, and wet years.

3.1.2 Reservoir Hydropower Plants

For reservoir-based plants, inflow is divided into storable and non-storable components based on the reservoir's filling time. The storable component, which equals the reservoir's live storage volume (i.e., 70% of total reservoir volume), is distributed evenly across seasons. The non-storable component, which exceeds the live storage volume, is assumed to be directly turbined. For reservoirs with a filling time longer than one year, the non-storable component is considered equal to zero. Since the filling time can be different in dry, normal and wet conditions, a reservoir's non-storable component varies depends on the hydrologic conditions and, for example, might be zero in dry years only.
Total outflow is the sum of these two components. The capacity factor profiles are then derived from these outflow profiles as described in the previous section.

3.1.3 Cascade Configurations

Cascade configurations involve one or more run-of-river or small reservoir plants downstream of larger reservoir plants. The inflow profile for the first downstream plant equals the outflow profile of the upstream reservoir plant, and this pattern continues downstream. Outflow profiles are converted to capacity factors using the equations described before. The impact of new upstream reservoirs on existing downstream plants is also considered.
Since cascade configurations can be time-dependent – i.e., a reservoir plant may be planned or under construction upstream of an existing run-of-river plant - cascade configurations are evaluated for specific years (2020, 2030) and hypothetical scenarios where all planned plants are operational.

3.2 Numerical Results

The capacity factors for all hydropower plants included in the African Hydropower Atlas (i.e., existing, committed, planned and candidate projects) are first computed over the historical time period (1980-2016). In the original implementation of the OsEMOSYS-TEMBA model, all hydropower plants have a nominal capacity factor equal to 0.5. Our estimates suggest water availability substantially limit hydropower generation: in normal conditions, the

average capacity factor of 64% of the modelled plants (405 out of 633) is lower than 0.5. The spatial distribution of these capacity factors (Figure 8) highlights diverse patterns with the Nile River Basin emerging as a region with high (dark green) capacity factors; conversely, the large majority of the hydropower plants in West Africa is characterized by low (dark purple) capacity factors. Many hydropower plants in Southern Africa also have relatively low (light purple) capacity factors. This spatial variability suggests hydropower can contribute differently across the five power pools, emphasizing the limitation of the current assumption of a homogeneous capacity factor equal to 0.5.

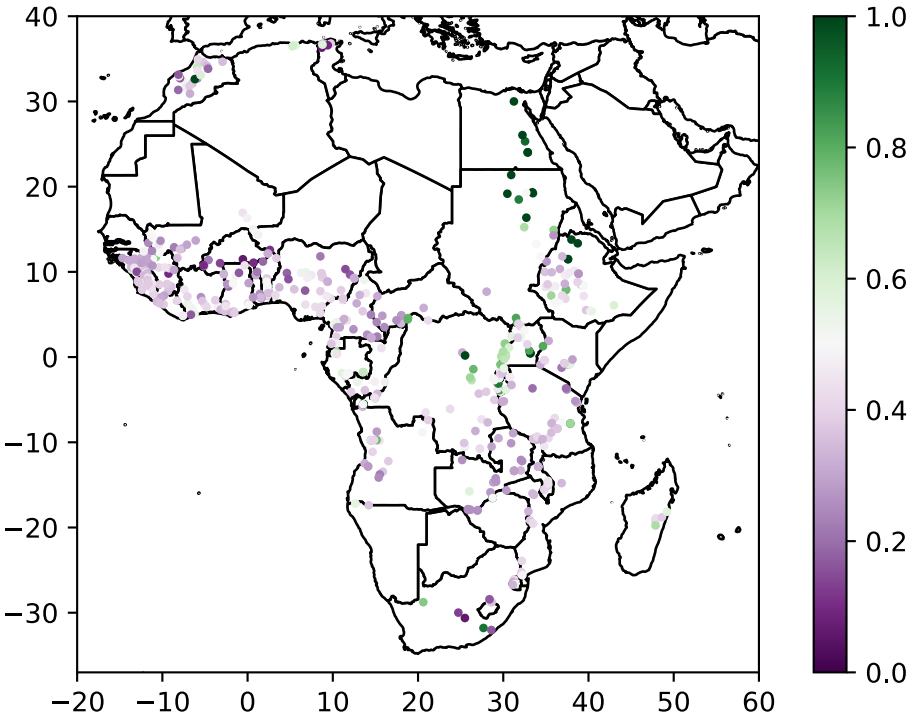

Figure 8: Average capacity factors for the hydropower plants in the African Hydropower Atlas conditioned on the water availability simulated by SWAT+ in normal hydrologic conditions. The nominal capacity factor of these plants in the OsEMOSYS-TEMBA model is 0.5.

In addition to the heterogeneity of the average capacity factors in normal conditions illustrated in Figure 8, hydropower generation varies because of intra-annual and inter-annual hydrologic variability. To investigate these aspects, Figure 9 compares the normal, dry and wet monthly capacity factors for the Kariba and Kafue Gorge hydropower plants in the Zambezi Watercourse. Results show how the large storage capacity of Kariba makes its hydropower plant insensitive to the intra-annual hydrologic variability, allowing a constant generation over the months of the year. Conversely, the smaller capacity of Kafue Gorge reservoir makes the generation more sensitive to monthly water availability, with the estimated capacity factor that is higher in the wet season (i.e., January-February-March) and lower in the rest of the year.

Both power plants show a pronounced sensitivity to inter-annual variability, with large differences between the normal, dry and wet capacity factors. In wet conditions, Kariba increases from 0.18 to 0.7, while it drops to 0.01 in dry conditions. Similarly, Kafue Gorge in the wet season fluctuates from 0.52 in normal conditions to 1.0 or 0.09 in wet and dry

conditions, respectively. These findings showcase the strong limitations of assuming a constant capacity factors for modeling the hydropower generation in energy systems models.

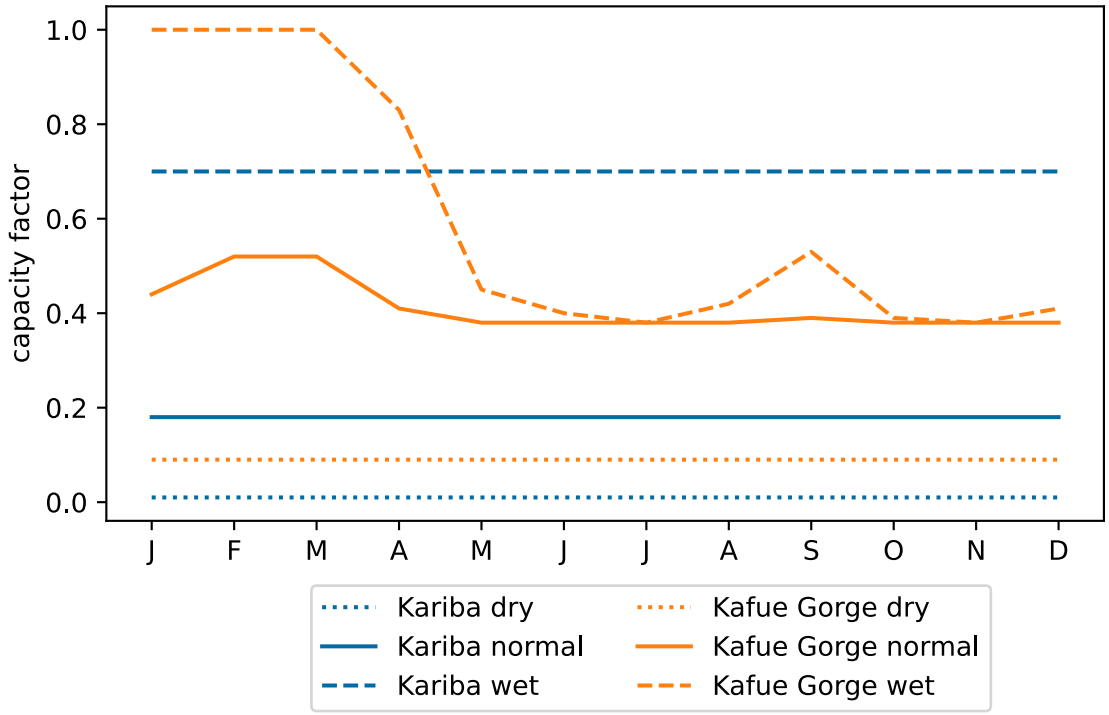

Figure 9: Monthly capacity factors for Kariba and Kafue Gorge power plants in the Zambezi Watercourse for different hydrologic conditions over the period 1980-2016.

Finally, building on these results we investigated the potential variability of the capacity factors across different future scenarios, namely SSP1-RCP2.6, SSP4-RCP6.0 and SSP5-RCP8.5. Specifically, we simulated the projected hydrological conditions over the time period 2020-2050 using the SWAT+ model with inputs derived from bias-adjusted projections of four global climate models (GFDL-ESM2M, HadGEM2-ES, ISPL-CM5A-LR, and MIROC5) forced with the concentration described in the Representative Concentration Pathways (RCPs) associated to each of the SSP scenarios part of the ISIMIP2b project. Figure 10 provides an example of results using the Manantali power plant in the Senegal River Basin. Results suggest that inter-annual variability is more impacting than the three scenarios. The wet and dry capacity factors are very similar under the SSP1-RCP2.6 and SSP4-RCP6.0 scenarios, while being slightly reduced under the SSP5-RCP8.5 one. In normal conditions, the projected capacity factor under the SSP1-RCP2.6 scenario is instead slightly higher than under the other two scenarios. In particular, the monthly capacity factors under SSP1-RCP2.6 are always higher than 0.6, while they vary between 0.51 and 0.63 under the other two scenarios. Considering again the nominal and constant capacity factor equal to 0.5 implemented in OSeMOSYS-TEMBA, our findings suggest the need of linking them to projected water availability for properly representing the contribution of hydropower technology to the future energy transition.

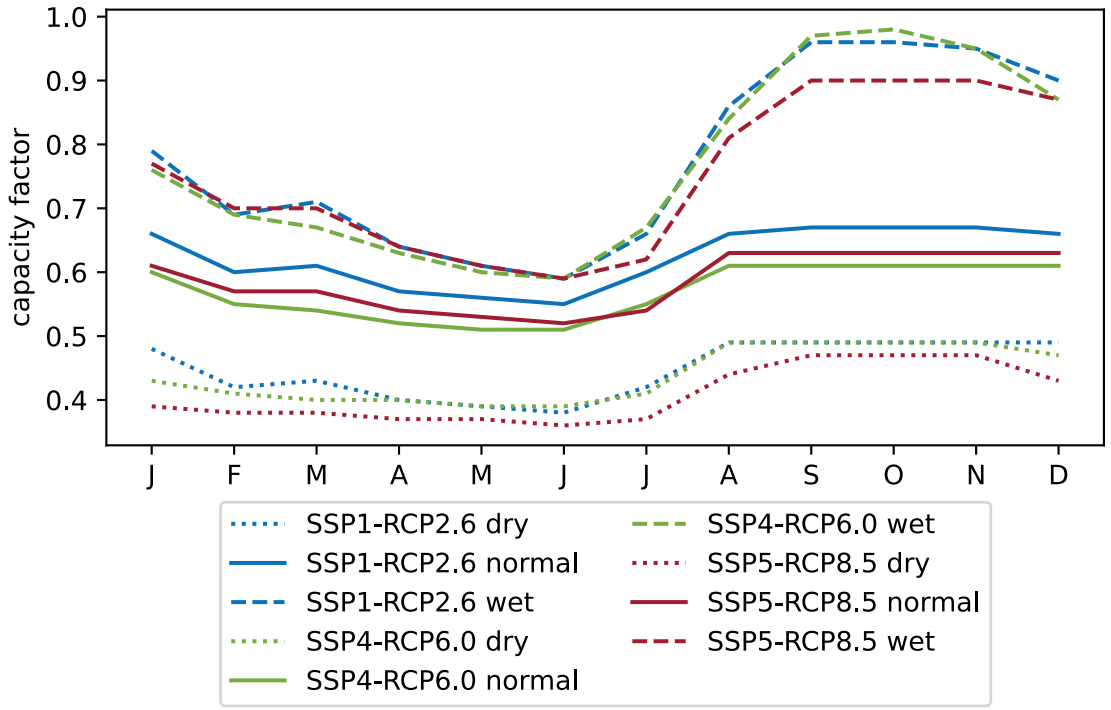

Figure 10: Monthly capacity factor for the Manantali power plant in the Senegal River Basin under different SSP-RCP projections over the period 2020-2050 and for different hydrologic conditions.

4 Political Instability and its Influence on Power Trade Vulnerability in Africa

In the context of global policies for climate change mitigation on the energy sector (IPCC, 2023), the African continent represents a critical juncture, especially for the possible side effects of the energy transition at the local scale. Despite its traditional reliance on fossil fuels (IRENA, 2024), Africa's abundant renewable energy resources (IRENA, 2022) offer significant potential for bypassing carbon-intensive technologies and achieving a net-zero energy sector while promoting socio-economic development. Although Africa contributes only 3.8% of global GHG emissions (CDP, 2020), its growing population and increasing incomes are projected to drive up demand for modern energy by one-third between 2020 and 2030 (IEA, 2022). However, meeting the United Nations Sustainable Development Goal (SDG) of universal access to modern energy by 2030 (SDG7) (UN, n.d.) remains a formidable challenge, as 600 million people in Sub-Saharan Africa still lack access to modern, reliable, and clean energy in 2022 (IEA, 2023).

Despite the opportunities for an energy transition, Africa faces numerous context-specific challenges. High levels of corruption, political instability, and ineffective governmental institutions (Kaufmann, 2023), especially in Central African nations, deter foreign investment in the continent's renewable energy potential (Komendantova et al. 2012). Furthermore, political violence and armed conflicts (ACLED, n.d.) threaten national energy security, with power outages often increasing during times of conflict (Spyrou et al. 2019). Power infrastructure, such as transmission lines, is particularly vulnerable to destructive attacks (EIAD, n.d.) (Zerriffi et al., 2002) as evidenced during the Mozambican civil war in 1992 (ECA, 2009) and recent vandal attacks in Kenya (Alushula, 2023), Nigeria (The Guardian Nigeria, 2024), and Uganda (Otage, 2022). In addition to electricity supply, fuel supply is also at risk due to political disputes, such as the recent conflict between Uganda and Kenya that jeopardized Uganda's fuel imports ("Kenya Ends Oil Import Feud with Uganda," 2024; Rukanga, 2023).

Traditional large-scale energy system planning often overlooks energy security and governance issues, which are crucial in unstable political contexts (O Dioha et al. 2023). Policymakers typically focus on least-cost energy system models emphasizing techno-economic factors, neglecting the environmental and socio-political implications of the energy transition. Although some models incorporate climatic objectives through emission constraints or multi-objective optimization (Zeng et al. 2011), few studies explicitly evaluate the socio-political implications of the energy transition (Trotter et al. 2018) (Freeman, 2021) (Korkovelos et al. 2020) or the disruptions caused by political instability (Patankar et al. 2019).

Moreover, the uncertainty of future socio-economic and climatic conditions complicates large-scale energy systems planning, affecting predictions of future energy demand and renewable energy availability. Hydropower production, for example, is highly dependent on climatic conditions (Wasti et al. 2022). Scenario analysis, using Shared Socio-economic Pathways (SSPs) (Bauer et al. 2017) and Representative Concentration Pathways (RCPs) (Van

Vuuren et al. 2011), can address some of these uncertainties by planning energy system capacity expansions under various future scenarios.

This study fits into the broader discussion on the side effects of global policies on local multisector dynamics by evaluating how continental energy transition strategies, designed with a least-cost approach, are impacted by local socio-political instability. The research focuses on continental Africa, examining cost-optimal power trade strategies under different socio-economic and hydro-climatic scenarios. By identifying which time frames, geographic areas, and scenario assumptions are associated with significant risk variations, this study aims to provide policymakers with insights into how global energy policies might influence local energy security, socio-political stability, and overall development. This approach highlights the need for more nuanced energy planning that integrates socio-political factors and addresses the potential unintended consequences of global policies at the local level.

The energy systems modelling framework employed for this work is OSeMOSYS -TEMBA AHA (Carlino et al., 2023), an open-source optimization model for energy generation and supply in 48 African countries. It integrates the African Hydropower Atlas (Sterl et al., 2022) to include capacity factors for 633 (existing or planned) hydropower projects. We solved the model considering three socio-economic and climatic scenarios, obtained by coupling Shared Socio-economic Pathways (SSPs) (Bauer et al. 2017) (Riahi et al., 2017) and Representative Concentration Pathways (RCPs) (Van Vuuren et al. 2011). The model was solved by coupling each socio-economic and climatic scenario with the two hydrological regime scenarios. Therefore, this approach yielded six cost-optimal strategies for the African energy sector, spanning the period from 2015 to 2050.

We then evaluated the vulnerability of the cost-optimal energy strategies through a measure of the power trade-related political risk (Trotter et al. 2018), quantifying the susceptibility of electricity exchanges to disruptions due to the instability of the countries involved. We performed the analysis both at the continental and at the national scale, considering countries' governance indicators coherently projected with each SSP (Andrijevic et al., 2019). From the findings, we tracked the temporal evolution of continental political risk over the upcoming decades across the different scenarios. We pinpointed countries that could be potential hotspots of political risk and assessed the differentiated impacts of socio-economic and climatic scenarios as well as the occurrence of droughts. Finally, we stochastically quantified potential power deficits arising from deviations in cost-optimal international power trades caused by political instability. The analysis assumes that countries with unstable governments, corruption, and/or frequent armed conflicts may deviate from the optimal level of power trade at the continental power system level. This approach allowed us to identify temporal and spatial criticalities, as well as scenario assumptions that could significantly impact energy security.

4.1 Methodology

4.1.1 OSeMOSYS TEMBA AHA

The modelling framework employed for this work is OSeMOSYS-TEMBA AHA (Carlino et al., 2023). It is based on OSeMOSYS –TEMBA ("OSeMOSYS - TEMBA," n.d.), a regional version of the global model, OSeMOSYS Global ("OSeMOSYS," n.d.) (Barnes et al., 2022), representing the electricity generation and supply system for 48 African countries. It is an open-source optimisation model that finds the least-cost energy generation, capacity expansion and transmission strategies, based on energy sources availability, to satisfy given trajectories of energy demand over time. To improve the level of detail used in its representation of hydropower plants, the model was integrated with the African Hydropower Atlas (AHA) (Sterl et al., 2022), a database collecting information on the capacity factors of 633 existing and planned hydropower projects in Africa.

4.1.1.1 Scenario definition

Energy demand definition in OSeMOSYS-TEMBA AHA was based on scenarios from the Inter-Sectoral Impact Model Intercomparison Project (ISIMIP2b) (Frieler et al. 2017). These scenarios are commonly used to coherently consider future final energy demands, land-use changes, and climate impacts on the hydrological cycle. Within each ISIMIP2b scenario, the definition of the energy demand is based on a single Shared Socio-economic Pathway (SSP) (Riahi et al., 2017), describing future socio-economic and political environment. Within ISIMIP2b, each SSP also is associated to a Representative Concentration Pathway (RCP) (Van Vuuren et al. 2011), describing a radiative forcing trajectory that is associated with a specific mitigation effort.

All SSP-RCP combinations, therefore, reflect specific levels of challenges to adaptation, challenges to mitigation and actual efforts for climate change mitigation at the global scale. The three scenarios considered for this study are:

- **SSP1-2.6 ("Sustainability" scenario)**: accounts for sustainable development and constrained carbon emissions, in a global effort to limit long-term global warming to 2°C,
- **SSP4-6.0 ("Inequality" scenario)**: focuses on heterogeneous economic development among regions and is not associated with specific climate mitigation efforts,
- **SSP5-8.5 ("Fossil-fueled development" scenario)**: accounts for high fossil-fuelled economic growth and is therefore associated with high greenhouse gas emissions.

The final energy demands in this study were obtained by combining energy demand projections available in OSeMOSYS-TEMBA with SSP-informed projections, considering that the earlier are more reliable in the short term while the latter are more relevant in the long term.

4.1.1.2 African Hydropower Atlas

In the African Hydropower Atlas (Sterl et al., 2022) historical capacity factors for existing hydropower projects are estimated monthly via the hydrological model SWAT+ ("SWAT+," n.d.). Meteorological data cover the 1980-2016 time period. Capacity factor projections over the 2020-2050 time period are also available in AHA. They were obtained for the three ISIMIP2b scenarios using as input bias-adjusted projections from four global climate models, forced with the RCPs associated to each SSP.

Capacity factors in AHA also reflect different hydrological regime, as they are based on inflow profiles for each month under normal, very wet, and very dry conditions. Normal capacity factors are derived as monthly median, while very wet and very dry are obtained by multiplying the monthly median profiles by the ratio of 5th and 95th percentile of annual generation to multi-annual average generation. For the purpose of this study, normal and very dry scenarios were considered. Specifically, the latter serve to account for risk-aversion of policymakers to drought events.

4.1.2 Continental power trade-related political risk

The evaluation of the political risk associated with the cost-optimal energy strategies is based on the work by Trotter et al. (Trotter at al. 2018). The study provides a formulation of the preventable political risk at the network level, defined as the political risk that can be avoided by designing the energy network differently. In Trotter's work, the risk is obtained as a linear combination of six factors, each describing a different driver of risk. However, a preliminary calculation of the different factors, conducted on the optimal strategies obtained from our model optimisation, showed that only three of them have a significant impact on the overall political risk (contributing to more than 90% of the total risk on average). Thus, for the calculation of the network-level political risk, our work focuses its attention only on three said factors, disregarding the non-relevant ones.

The relevant factors in question characterise different dimensions of risk that arise when energy exchanges are carried out between unstable countries. The total amount of exported power in the network is weighted on the governance performance of countries that carry out such trades. Each of the three risk factors refers to a different dimension of countries' governance: the efficacy of their political institutions, their degree of political instability and their level of interference of private political interests in policy decisions. The characterisation of countries' governance performance is based on World Bank's Worldwide Governance Indicators (WGI) (Kaufmann, 2023) and on the degree of autocracy obtained from the Polity IV scale (Marshall et al. 2015). The firsts were projected to 2050 according to the SSP assumptions behind every scenario.

Variables

- $d\ in\ D$: demand node - 48 electricity-demanding nodes in the network,
- $g\ in\ G$: generation technology - 10 generation technologies (biomass, solar PV, wind, hydro, geothermal, coal, oil, gas, fuel oil, nuclear),
- $s\ in\ S$: supply node - 48 electricity-supplying nodes in the network,
- $t\ in\ T$: time period - 36 time periods corresponding to years from 2015 to 2050,
- x_{sdgt}: decision variable describing the amount of electricity produced at supply node s, by generation technology g, in year t, and sent to demand node d (in GWh).

Network-level formulation

This risk formulation is intended to obtain a yearly risk evaluation at the continental level, aggregated for all countries in the network.

1) $$PolRisk_t = w_{PR3} \cdot PR3InstEffic_t + w_{PR4} \cdot PR4PolInst_t + w_{PR5} \cdot PR5PolInterest_t$$

$$\forall t \in T$$

Where:

2) $$\sum_{i=3}^{5} w_{PR_i} = 1$$

PR3InstEfficSup - Efficacy of political institutions

Political risk associated with a network relying on electricity exports produced in countries with poor political institutions. Its theoretical value is equal to 100 if all the demand in the network is generated in countries with lowest possible institutional capacities and full autocracies. It approaches 0 if all exported electricity is generated in countries with extremely strong institutions, or if no electricity is exported.

3) $$PR3InstEfficSup_{st} = \left(\frac{InstIneffect_s + Autocracy_s}{2} \right) \cdot \sum_{s \neq d} \sum_{g \in G} x_{sdgt}$$

$$\forall s \in S, t \in T$$

4) $$PR3InstEffic_t = \frac{\sum_{s \in S} PR3InstEfficSup_{st}}{\sum_{d \in D} demand_{dt}}$$

$$\forall t \in T$$

5) $$PR3InstEfficSup_{st} \in R_{\geq 0}, PR3InstEffic_t \in R_{\geq 0} \ \forall s \in S, t \in T$$

$InstIneffect_s$: Degree of institutional ineffectiveness in country s on a 0 – 100 scale, transformed from WGI Government Effectiveness index (Kaufmann, 2023).

$Autocracy_s$: Degree of autocracy in country s on a 0 – 100 scale, transformed from the Polity IV scale (Marshall and Jaggers, 2015) (from -10, full autocracy, to 10, full democracy).

Both $InstIneffect_s$ and $Autocracy_s$ have been calculated as 10-year averages between 2005 and 2014.

PR4PolInst - Political instability

Political risk of a network relying on politically unstable countries for electricity exports.

6) $$PR4PolInstSup_{st} = PolInst_s \cdot \sum_{s \neq d} \sum_{g \in G} x_{sdgt}$$

$$\forall s \in S, t \in T$$

7) $$PR4PolInst_t = \frac{\sum_{s \in S} PR4PolInstSup_{st}}{\sum_{d \in D} demand_{dt}}$$

$$\forall t \in T$$

8) $$PR4PolInstSup_{st} \in R_{\geq 0}, PR4PolInst_t \in R_{\geq 0} \ \forall s \in S, t \in T$$

$PolInst_s$: Degree of political instability in country s on a 0 – 100 scale, transformed from WGI Political Stability and Absence of Violence index (Kaufmann, 2023), calculated as average between 2005 and 2014.

PR5PolInterest - Private political interests

Political risk of a network relying on electricity exports from countries characterised by private political interference in policy decisions and implementation.

9) $$PR5PolInterestSup_{st} = Corruption_s \cdot \sum_{s \neq d} \sum_{g \in G} x_{sdgt}$$

$$\forall s \in S, t \in T$$

10) $$PR5PolInterest_t = \frac{\sum_{s \in S} PR5PolInterestSup_{st}}{\sum_{d \in D} demand_{dt}}$$

$$\forall t \in T$$

11) $$PR5PolInterestSup_{st} \in R_{\geq 0}, PR5PolInterest_t \in R_{\geq 0} \ \forall s \in S, t \in T$$

$Corruption_s$: Degree of corruption in country s on a 0 – 100 scale, transformed from WGI Control of Corruption index (Kaufmann, 2023).

4.1.2.1 Country-level power trade-related political risk

To identify regional hotspots of political risk in Africa, we also defined a country-level formulation of political risk. Each of the relevant continental risk factors described above was declined into two country-level factors: one considering power imports and one considering power exports. The six defined factors were combined linearly, with equal weights, to obtain the total country-level political risk.

This risk formulation provides the yearly risk calculation for each country in the network. Each country is represented by both a supply and demand node, but based on the specific risk formulation, it may be considered as either one of the two or both.

$c\ in\ C$: country - 48 countries in the network, each associated to a supply and demand node.

For the definition of all other variables refer to section 4.1.2.

12) $$PolRisk_{ct} = w_{PR3} \cdot PR3InstEfficSup_{ct} + w_{PR4} \cdot PR4PolInstSup_{ct} + w_{PR5} \cdot PR5PolInterestSup_{ct} + w_{PR6} \cdot PR6InstEfficDem_{ct} + w_{PR7} \cdot PR7PolInstDem_{ct} + w_{PR8} \cdot PR8PolInterestDem_{ct}$$
$$\forall c \in C, t \in T$$

Where:

13) $$\sum_{i=3}^{8} w_{PR_i} = 1$$

PR3InstEfficSup - Efficacy of political institutions (exports)

Political risk of a country relying on electricity exports towards countries with poor political institutions.

Its theoretical value is equal to 100 if all the supply country's generation is exported towards countries with lowest possible institutional capacities and full autocracies. It approaches 0 if all the supply country's exports are towards countries with extremely strong institutions, or if no electricity is exported.

14) $$PR3InstEfficSup_{st} = \frac{\sum_{d \neq s} \left(\left(\frac{InstIneffect_d + Autocracy_d}{2} \right) \cdot \sum_{g \in G} x_{sdgt} \right)}{\sum_{s=d} \sum_{g \in G} x_{sdgt}}$$

15) $$PR3InstEfficSup_{ct} = PR3InstEfficSup_{st}$$
$$\forall t \in T$$

16) $$PR3InstEfficSup_{st} \in R_{\geq 0}, PR3InstEfficSup_{ct} \in R_{\geq 0} \ \forall s \in S, c \in C, t \in T$$

PR4PolInstSup - Political instability (exports)

Political risk of a country relying on politically unstable countries for electricity exports.

Its theoretical value is equal to 100 if all the supply country's generation is exported towards countries with highest possible political instability. It approaches 0 if all the supply country's exports are towards countries with extremely high political stability, or if no electricity is exported.

17) $$\mathrm{PR4PolInstSup_{st}} = \frac{\sum_{d \neq s}\left(\mathrm{PolInst_d} \cdot \sum_{g \in G} \mathrm{x_{sdgt}}\right)}{\sum_{s=d} \sum_{g \in G} \mathrm{x_{sdgt}}}$$

18) $$\mathrm{PR4PolInstSup_{ct}} = \mathrm{PR4PolInstSup_{st}}$$
$$\forall t \in T$$

19) $$\mathrm{PR4PolInstSup_{st}} \in \mathrm{R_{\geq 0}}, \mathrm{PR4PolInstSup_{ct}} \in \mathrm{R_{\geq 0}} \quad \forall s \in S, c \in C, t \in T$$

PR5PolInterestSup - Private political interests (export)

Political risk of a supply country relying on electricity exports from countries characterised by private political interference in policy decisions and implementation.

Its theoretical value is equal to 100 if all the supply country's generation is exported towards countries with highest possible corruption levels. It approaches 0 if all the supply country's exports are towards countries with low corruption, or if no electricity is exported.

20) $$PR5PolInterestSup_{st} = \frac{\sum_{d \neq s}\left(Corruption_d \cdot \sum_{g \in G} x_{sdgt}\right)}{\sum_{s=d} \sum_{g \in G} x_{sdgt}}$$

21) $$PR5PolInterestSup_{ct} = PR5PolInterestSup_{st}$$
$$\forall t \in T$$

22) $$PR5PolInterestSup_{st} \in R_{\geq 0}, PR5PolInterestSup_{ct} \in R_{\geq 0}$$
$$\forall s \in S, c \in C, t \in T$$

PR6InstEfficDem - Efficacy of political institutions (imports)

Political risk of a country relying on electricity imports towards countries with poor political institutions.

Its theoretical value is equal to 100 if all the demand country's energy requirement is imported from countries with lowest possible institutional capacities and full autocracies. It approaches 0 if all the demand country's imported electricity comes from countries with extremely strong institutions, or if no electricity is imported.

$$PR6InstEfficDem_{dt} = \frac{\sum_{s \neq d}\left(\left(\frac{InstIneffect_s + Autocracy_s}{2}\right) \cdot \sum_{g \in G} x_{sdgt}\right)}{demand_{dt}}$$

24) $$PR6InstEfficDem_{ct} = PR6InstEfficDem_{dt}$$
$$\forall t \in T$$

25) $PR6InstEfficDem_{dt} \in R_{\geq 0}, PR6InstEfficDem_{ct} \in R_{\geq 0} \ \forall d \in D, c \in C, t \in T$

PR7PolInstDem - Political instability (imports)

Political risk of a country relying on politically unstable countries for electricity imports.

Its theoretical value is equal to 100 if all the demand country's energy requirement is imported from countries with highest possible political instability. It approaches 0 if all the demand country's imported electricity comes from countries with extremely high political stability, or if no electricity is imported.

26) $$PR7PolInstDem_{dt} = \frac{\sum_{s \neq d}\left(PolInst_s \cdot \sum_{g \in G} x_{sdgt}\right)}{demand_{dt}}$$

27) $$PR7PolInstDem_{ct} = PR7PolInstDem_{dt}$$
$$\forall t \in T$$

28) $PR7PolInstDem_{dt} \in R_{\geq 0}, PR7PolInstDem_{ct} \in R_{\geq 0} \ \forall d \in D, c \in C, t \in T$

PR8PolInterestDem - Private political interests (import)

Political risk of a supply country relying on electricity imports from countries characterised by private political interference in policy decisions and implementation.

Its theoretical value is equal to 100 if all the demand country's energy requirement is imported from countries with highest possible corruption levels. It approaches 0 if all the demand country's imported electricity is coming from countries with low corruption, or if no electricity is imported.

29) $$PR8PolInterestDem_{dt} = \frac{\sum_{s \neq d}\left(Corruption_s \cdot \sum_{g \in G} x_{sdgt}\right)}{demand_{dt}}$$

30) $$PR8PolInterestDem_{ct} = PR5PolInterestDem_{dt}$$

$$\forall t \in T$$

31) $$PR8PolInterestDem_{dt} \in R_{\geq 0}, PR8PolInterestDem_{ct} \in R_{\geq 0}$$

$$\forall d \in D, c \in C, t \in T$$

4.1.2.2 Governance indicators projections

The projection of governance indicators to 2050, in alignment with the SSP assumptions, was performed according to the methodology described by Andrijevic et al. (Andrijevic et al., 2019). In that work, the aggregate governance indicator from the WGI database is predicted according to GDP per capita, share of population with higher education and gender gap in mean years of schooling. The model is calibrated using country-level governance data from 1995 to 2015. Governance projections are obtained imposing coefficients estimated on historical data on projections of GDP, education and gender gap in education that are consistent with SSP projections.

The aggregate WGI indicator incorporates six dimensions of governance. For our political risk formulation, only three of them are relevant: Government Effectiveness, Political Stability and Absence of Violence and Control of Corruption. Therefore, the approach used by Andrijevic et al. on the aggregate governance indicator was replicated only on such relevant factors. Historical time series of each indicator were used to calibrate the model and the estimated coefficients were imposed on the above-mentioned projected socio-economic variables.

4.1.2.3 Power deficit calculation

We assume that future national decision-makers would determine the amount of energy to be exchanged with neighbouring countries following a cost-minimization perspective. In that case, the amount of energy to be exchanged between two countries, in a given year and on a given transnational transmission line, is assumed to be equal to the optimal amount obtained from our least-cost energy systems model. In this framework, we suppose that countries characterised by unstable governmental institutions, corruption and/or frequent armed conflicts may deviate from the level of power trade exchange which is optimal at the level of the continental power system. Therefore, we reduce the amount of energy exchanged on each transmission line by a deviation factor that depends, in a stochastic way, on the degree of instability of the energy exporter.

The methodology employed for this analysis stems from the work by Gold et al. (Gold et al., 2019), analysing the impact of operational deviations on the robustness of regional water supply portfolios. Adapting such methodology to this case study, the procedure employed consists in the implementation of a tolerance analysis, which includes:

1. the sampling of plausible stochastic operational deviations from the cost-optimal energy exchange strategies,
2. the evaluation of the vulnerability of cost-optimal solutions via calculation of yearly energy demand deficits.

Problem formulation

In this analysis, the cost-optimal amount of energy to be exchanged on a given transmission line in a given year, $\theta_{i,t}$, is perturbed through a multiplicative deviation factor, δ_c, depending on the degree of political instability (as defined for the political risk evaluation) of c, the exporting country on transmission line i.

32) $$\varepsilon_{i,t} = \theta_{i,t} \cdot \delta_c$$

$$\forall i \in I, t \in T$$

$\varepsilon_{i,t}$: reduced amount of energy exchanged on transmission line i in year t.
$\theta_{i,t}$: cost-optimal amount of energy exchanged on transmission line i in year t.
δ_c: deviation factor (0-1) associated to c, exporting country on transmission line i.

The determination of the deviation factor is performed in a stochastic way. To define this methodology, we started by the characterisation of a simple deterministic rule, associating different ranges of countries' political instability (calculated by averaging the dimensions of governance considered in the definition of political risk) to single, fixed values of operational deviation factors. The rule considered associates more unstable countries to more severe operational deviations, in a worst-case scenario perspective. This approach was then expanded by associating, to the same ranges of countries' political instability, not a single deterministic operational deviation factor, but a range of values that the factor could take. More specifically, each political instability range was associated to an operational deviation ranging from a minimum value $\delta_{c,min}$ (equal to the single value considered in the deterministic approach) to a maximum value $\delta_{c,max}$ (equal to one for all ranges). For each country in the network, according to its level of instability, was associated a numeric operational deviation sampled from the associated range.

Starting from this last approach, we obtained the definitive stochastic methodology by subjecting both the political instability ranges and the minimum deviation factors in sampling ranges, as previously defined, to a stochastic perturbation. The values of perturbation were sampled within a range that was defined through a sensitivity analysis, performed on the deterministic deficit in the Sustainability scenario. This sampling process was performed n = 100,000 times. By further increasing the number of samplings, no significant variations were obtained. In each of the samplings performed, a different deviation rule was stochastically defined, and each country was associated to a random operational deviation within the range defined by its degree of political instability. Then, for each transmission line between two countries, the reduced amount of power traded was obtained, from which it was possible to calculate the reduced imports and exports for each country in the network. This allowed to calculate the energy deficit associated to each country c in each sampling, according to the following formulation:

33) $$\Delta_{imports,\ c} = reduced\ imports_c - imports_c$$

34) $$\Delta_{exports,\ c} = reduced\ exports_c - exports_c$$

35) $$\Delta_c = \Delta_{imports,\ c} - \Delta_{exports,\ c}$$

36) $$deficit_{abs,\,c} = \Delta_c \quad if\ \Delta_c < 0$$

37) $$deficit_c\ [\%] = \frac{deficit_{abs,\,c}}{demand_c}$$

Lastly, the deficit obtained for each country was averaged over the n samplings. Further spatial and temporal aggregations were performed to analyse the obtained results.

4.2 Numerical Results

4.2.1 Increased energy demand causes surge in continental political risk in the first half of 2020-2030

Results reported in Figure 11 indicate that political risk at the continental level peaks in the first half of the 2020-2030 decade for all scenarios, subsequently decreasing steadily until 2050. In general, Sustainability scenarios display the highest levels of risk, followed by Inequality and Fossil-fueled development scenarios. Between 2045 and 2050 the risk in Inequality scenarios surpasses that in Sustainability scenarios. Near the peak, scenarios with very dry hydrology tend to show lower political risk compared to their analogous median hydrology scenarios. Moving towards 2050, this difference becomes less pronounced, and median hydrology scenarios often outperform very dry hydrology scenarios.

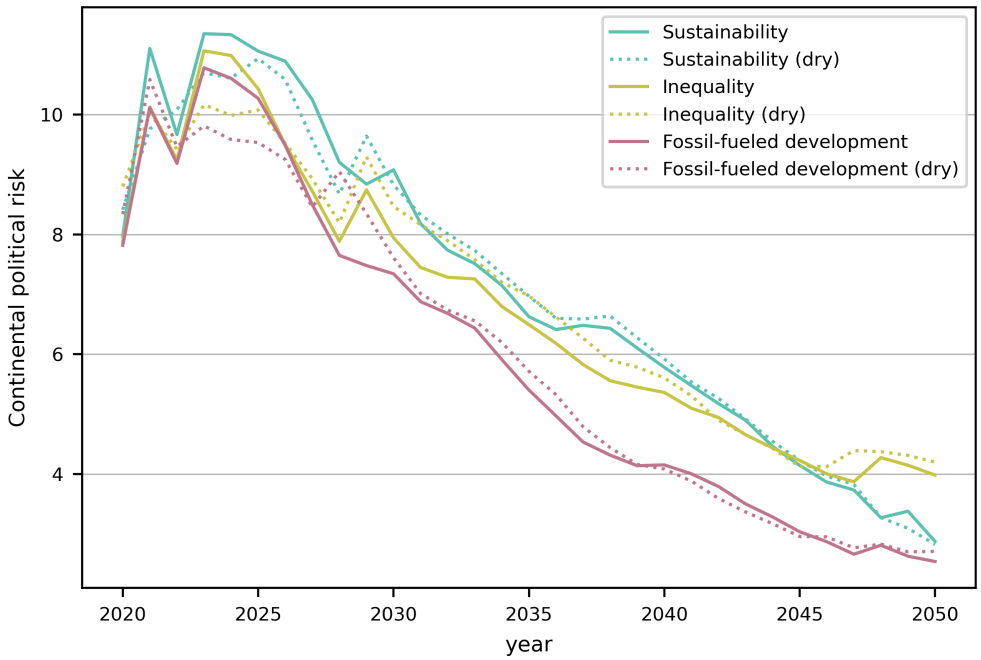

Figure 11: Continental political risk. Yearly values political risk for the entire African network under the six scenarios considered.

The surge in continental political risk between 2020 and 2030 can be attributed to the projected increase in demand for modern energy in Africa, driven by population and income growth. This demand is expected to rise by one-third between 2020 and 2030 (IEA, 2022). Initially, the model cannot cost-effectively meet the increased energy demand through countries' endogenous power generation, causing many countries in the network to rely heavily on energy exchanges during this initial phase. As the power system evolves, older power plants end their operational lifetime and new plants are constructed closer to demand centres. This reduces the role of transmission and, consequently, of power trade, which mitigates the risk associated with political instability.

These findings indicate that policymakers should take an active role in supporting African nations during their energy transition, particularly during this critical initial phase marked by heightened risks. Policies aimed at decreasing energy dependence should be prioritized. By promoting the diversification of energy sources, investing in renewable energy infrastructure, and fostering local energy production capabilities, policymakers can help mitigate the vulnerabilities associated with heavy dependence on energy exchanges and enhance the continent's resilience to political risks.

4.2.2 Country-level political risk hotspots located in western, southern and central-eastern Africa

Since the continental analysis indicated that the 2020-2030 decade is expected to be the most critical in terms of political risk, the quantification and analysis of country-level political risk focused primarily on this period. Specifically, Figure 12 displays the maximum levels of political risk registered for each country during 2020-2030 under different scenarios. The results indicate that political risk hotspots at the country level are primarily located in

western, southern, and central-eastern Africa. Notably, four countries exhibit very critical levels of risk (>100) across all scenarios: Guinea-Bissau, Liberia, Rwanda, and Togo.

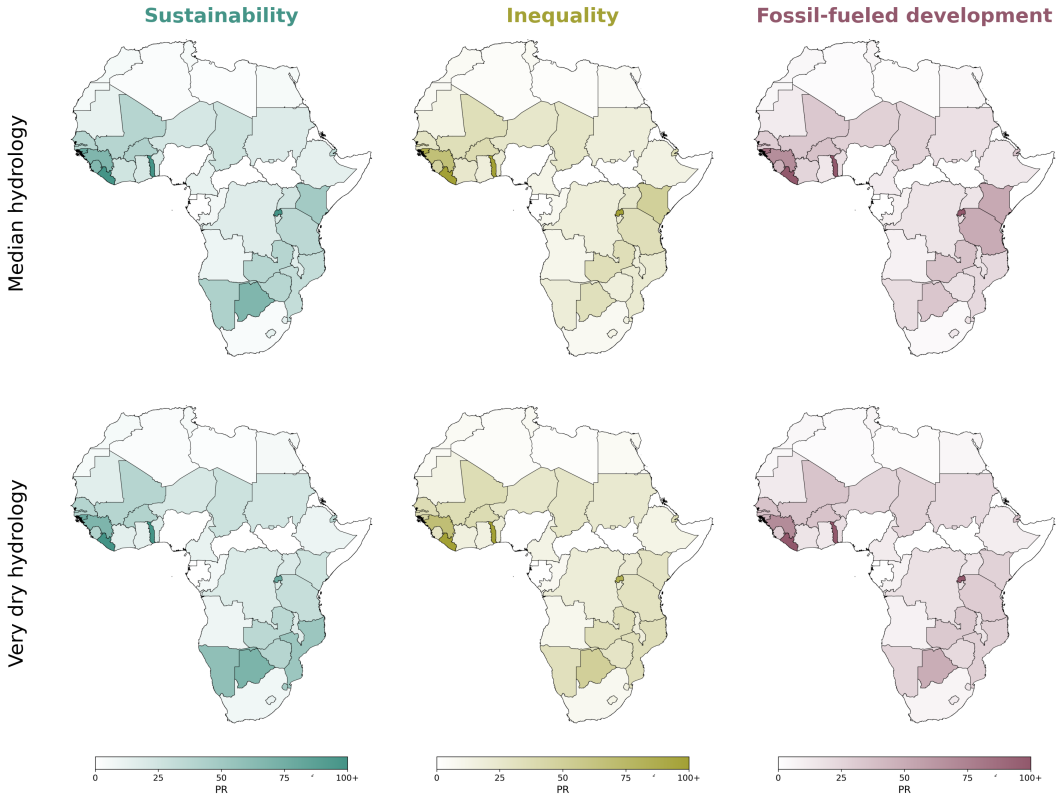

Figure 12: Maximum political risk for each country in the network in 2020-2030. This decade was deemed most critical based on continental risk analysis. In alignment with this worst-case approach, maximum risk values are shown.

These findings underscore the potential risks associated with already precarious energy security situations, particularly in Western Africa. For instance, Togo is characterized by significant power losses due to power thefts and aging infrastructure, while Liberia faces challenges related to unsafe petroleum product supply caused by political unrest, piracy, maritime boundary disputes, oil trafficking, and bunkering activities (Ofosu-Peasah et al. 2021). It is also known that Togo's energy supply is largely dependent on importation from neighbouring countries (Ajayi, 2013). These pre-existing conditions exacerbate the power trade-related political risk in these areas, which therefore need to be targets of interventions aimed at improving energy security and political stability.

Understanding the root causes of political risk in critical areas is essential for developing effective strategies to mitigate these risks. Countries such as Liberia, Togo, and Rwanda, which are characterized by critically high levels of political risk (>100), also show very high fractions of exported power over total generation and/or very high fractions of imported electricity over total demand during the same timeframes.

4.2.2.1 Country-Specific Scenario Adaptation Strategies and Political Risk Effects

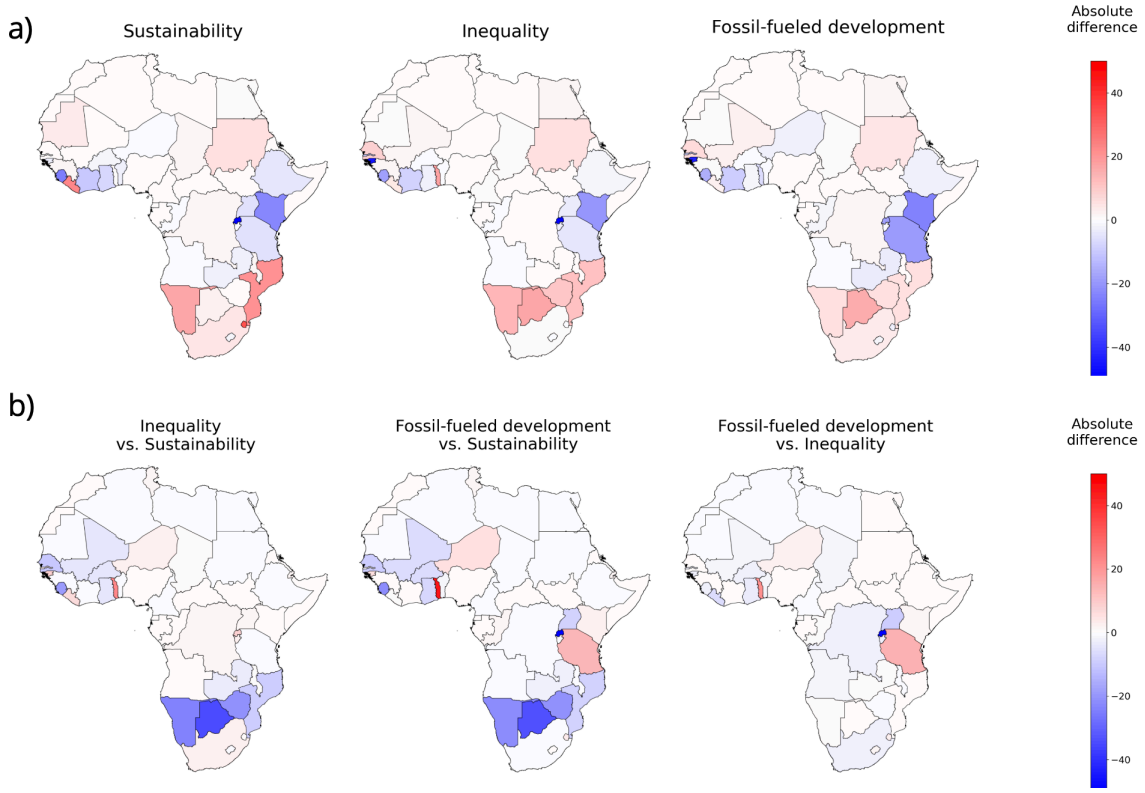

Figure 13: Country-level political risk variations. Obtained by subtracting: a) risk of median hydrology scenarios from risk of very dry hydrology scenarios (assuming same SSP-RCP) b) risk of more sustainable scenarios from risk of less sustainable scenarios (assuming median hydrology). Risk values refer to the maximum levels of political risk for each country in the network in 2020-2030 (displayed in fig. 6-2).

Our analysis reveals that the same scenario assumptions can produce different effects on African countries in terms of political risk, as each nation adapts its energy system expansion strategies, to meet projected energy demand trajectories, according to its specific energy resource availability. To assess how scenario assumptions influence political risk, we conducted a variation analysis. Figure 13 shows absolute variations in the maximum country-level political risk, during the 2020-2030 decade, between median and very dry hydrology scenarios. The results indicate that very dry hydrology scenarios are associated with increased political risk, particularly in southern Africa, compared to median hydrology scenarios.

For instance, drought events and decreased hydropower productivity compel countries in the Zambesi area, such as Mozambique, to reduce their reliance on hydropower for self-consumption. Consequently, they are forced to increase their reliance on imported electricity, leading to heightened political risk. For Namibia, the lost generation from hydropower is compensated through increased power production from solar and gas. Nevertheless, despite a general decline in energy exports, this fails to align with the reduced power generation. Consequently, the export-to-generation ratio escalates, leading to a greater dependence on electricity exports and thereby exacerbating political risk. As for Mozambique and Namibia, an energy mix heavily reliant on hydropower production can potentially heighten political risks during drought scenarios. However, this is not universally applicable, since not all nations with high proportions of hydropower in their energy

generation witness a significant decline in hydropower output during droughts (as, for instance, the Democratic Republic of Congo).

Conversely, countries that experience significant decreases in hydropower generation during droughts may not necessarily face heightened political risks as a result of increased energy imports. This dynamic is observed in the Nile River basin. Egypt, for instance, effectively manages this risk by ramping up solar power generation, thus diminishing its reliance on imports and exports. Likewise, Sudan and Ethiopia attain comparable results by expanding their utilization of natural gas. Conversely, Rwanda can successfully mitigate risk by more than halving its electricity exports through increased production from geothermal and solar sources. Kenya, by enhancing its wind energy production, can achieve a similar risk reduction. Therefore, while the relationship between very dry hydrology scenarios and political risk is significant, it is not uniform across all nations. Diversified energy mixes represent effective strategies for mitigating political risk. Understanding these dynamics is crucial for policymakers navigating the complexities of energy security and political stability in the face of hydrological uncertainties.

Similarly to the analysis of hydrological regime risk variation, we also examined the impact of socio-economic and climatic assumptions on political risk. Figure 13b illustrates the absolute variations in maximum country-level political risk, during the 2020-2030 decade, between more and less sustainable scenarios. Our findings reveal that Sustainability scenarios are associated with a slight increase in political risk, particularly noticeable in southern Africa compared to Inequality and Fossil-fueled development scenarios. However, in contrast to the comparison between the median and very dry hydrology scenarios, determining whether the variances in political risk stem from the socio-economic or the climatic assumptions within these scenarios is not feasible. It is more probable that the observed effects result from a blend of both sets of assumptions.

For instance, Namibia, Zimbabwe and Botswana exhibit notably lower risks in the Inequality and Fossil-fueled development scenarios compared to the Sustainability scenario. The socio-economic trajectories associated with the less sustainable scenarios are characterized by accelerated population growth, leading to heightened energy demands and subsequently increased power generation. However, in scenarios with less stringent climate regulations, these nations can meet the augmented energy requirements primarily through inexpensive fossil fuels (coal in Botswana's and Zimbabwe's case, and gas in Namibia's). The additional generation also serves to curtail their reliance on foreign energy imports and exports, thereby mitigating their political risk.

In this context, a notable anomaly arises with Togo, diverging from the continental trend by experiencing heightened political risk in less sustainable scenarios. The shift towards cheaper coal as an energy source in these scenarios prompts Togo to transition from minimal reliance on coal for energy production to sourcing over half of its energy mix from it. Conversely, gas, previously relevant in Togo's energy portfolio, diminishes substantially or entirely in less sustainable scenarios. The increased energy generation demanded by the socio-economic assumptions underpinning these scenarios also leads to a significant surge in both energy imports and exports for Togo. Once again, Togo emerges as a regional electricity dispatch

intermediary, utilizing its additional coal-based energy generation primarily for export purposes, which increase the country's exposure to trade-related political risk.

It is therefore crucial to account for the unique economic attributes and available resources of individual countries when examining the effects of climate change mitigation policies. Indeed, these unique attributes may result in diverse socio-political outcomes from such policies. The impacts largely depend on a nation's ability to adapt to changes in its economically viable energy supply mix. In the scenarios crafted for this study, the combination of SSPs and RCPs complicates the attribution of impacts on the individual assumption categories. Future research endeavours should concentrate on investigating the individual contribution of socio-economic and climatic assumptions on political risk variations. For instance, the well-established notion that climate policies can enhance energy security, leading to reduced dependence on energy imports (Clarke et al. 2022) (Cherp et al., 2016) (Jewell et al. 2013), should correlate, in such scenarios, with a decrease in political risks associated with power trade.

4.2.3 Poor governance performance is associated to more severe power deficits

The evaluation of continental power deficits due to operational deviations, whose results are summarized in Table 3, highlights that, in alignment with political risk, 2020-2030 is the most critical decade for power deficits. This holds true considering both average deficits, which don't exceed 1.3%, and maximum deficits, which don't exceed 12%. Moreover, Inequality scenarios display higher levels of deficit with respect to Sustainability and Fossil-fueled development scenarios. In alignment with the scenario comparison conducted on political risk, it remains challenging to definitively attribute the deficit disparities to either the socio-economic or the climatic assumptions behind our scenario definitions. Nevertheless, it is plausible to assert that the predominant driver of increased deficit in Inequality scenarios is the overall poorer governance status of African countries in those scenarios.

Table 3: Average and maximum continental power deficits due to operational deviations. Countries displaying maximum risk values are reported (LR = Liberia, ZM = Zambia, EG = Egypt, RW = Rwanda, CM = Cameroon).

		Sustainability				Inequality				Fossil-fueled development			
		Median		Very dry		Median		Very dry		Median		Very dry	
Average deficit	2020-2030	1.03%		1.01%		1.30%		1.14%		0.98%		0.85%	
	2030-2040	0.10%		0.11%		0.44%		0.44%		0.10%		0.12%	
	2040-2050	0.02%		0.02%		0.19%		0.18%		0.01%		0.01%	
	TOT	0.39%		0.38%		0.64%		0.59%		0.37%		0.33%	
Maximum deficit	2020-2030	LR	9.43%	LR	11.82%	LR	10.74%	ZM	10.28%	ZM	8.04%	ZM	9.22%
	2030-2040	ZM	1.47%	ZM	1.70%	RW	4.48%	ZM	4.66%	ZM	2.26%	ZM	2.40%
	2040-2050	EG	0.81%	EG	0.78%	CM	1.46%	ZM	1.45%	EG	0.42%	EG	0.34%

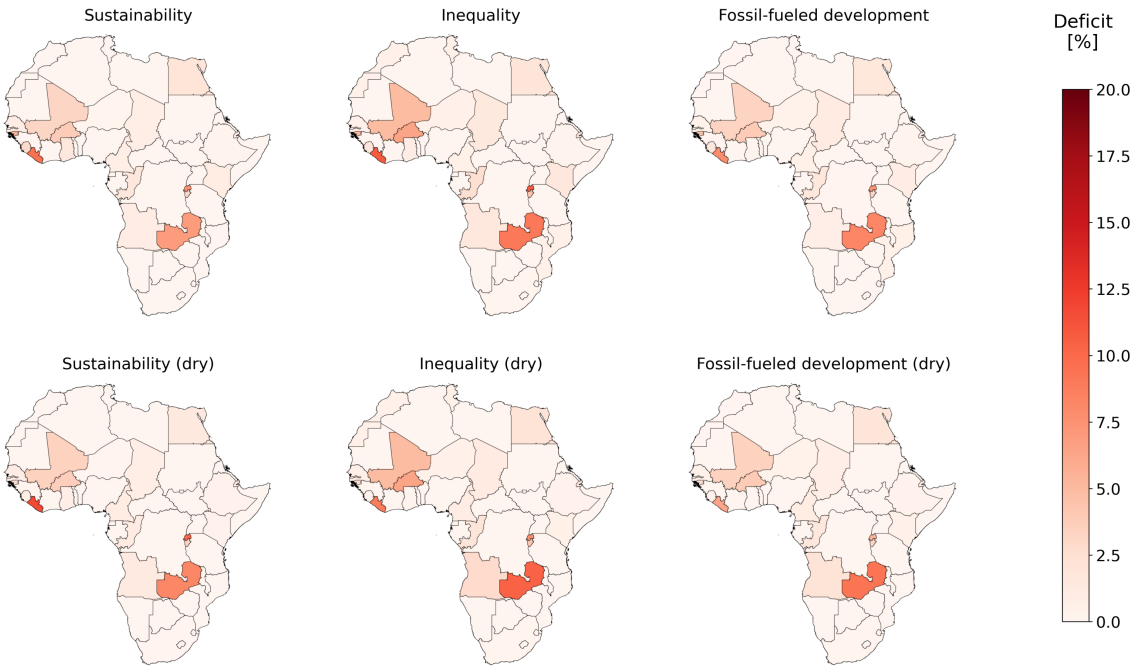

Figure 14: Average country-level power deficits due to operational deviations in 2020-2030. This decade was deemed most critical based on continental power deficit evaluation (tab. 1).

Figure 14, on the other hand, displays results from the country-level power deficit assessment. Results indicate that hotspots of deficit, during the most critical decade, would be mainly located in central and western Africa under all scenarios. Deficit hotspot locations show no evident regional overlap with political risk hotspots (Figure 13), except for some of the most critical countries, like Liberia and Rwanda. Specifically, Liberia, similarly to Togo, functions as a regional electricity dispatch intermediary, importing surplus power to be exported to its neighbouring countries. However, countries with whom Libera carries out energy exchanges (namely Côte d'Ivoire, Guinea, and Sierra Leone) face greater instability compared to Togo's (involved with Benin, Ghana, Niger, and Nigeria). Consequently, Liberia is more vulnerable to potential energy deficits despite sharing comparable levels of political risk with Togo. In general, countries characterised by high potential deficits are associated with either a power supply mix heavily dependent on energy imports and/or exports, or a regional framework marked by considerable and widespread political instability.

5 From multi-decadal energy planning to hourly power dispatch: evaluating the reliability of energy projections in the Southern African Power Pool

In developing countries, and particularly in the African continent, the energy transition has emphasized the urgency of expanding affordable and clean energy sources (IEA, 2022). In this context, energy system planning models, which solve cost-optimal trajectories of capacity expansion for different technologies, are key tools to assist the economic development in the poor regions (Dalla Longa and Van Der Zwaan, 2021) and to transit to a net zero emission energy system(Ou et al., 2021). However, they generally miss out on short-term but high-intensity events due to their limited spatio-temporal resolution. This limitation is evident in energy systems with non-dispatchable variable renewable energy resources (VRES), which rely on fluctuating external influences (Pfenninger et al., 2014). To address this challenge, an integration with power system models, which are used to balance electricity supply and demand with high temporal and spatial resolution, minimizing the cost of the grid, can offer a solution. Power systems are a component of energy systems, and they focus on a single energy carrier, i.e. they describe the process of generation and distribution of electricity. While energy system models identify technologies with the greatest impact on greenhouse gas emissions and the lowest technical financial risk, power system models address system reliability, as the share of VRES grows. The integration of energy system models with power system models is thus beneficial.

In this work, we integrate a long-term energy planning model, OSeMOSYS- TEMBA (Pappis et al., 2019), and a power system simulation model, PowNet (Chowdhury et al., 2020).The integration is carried out through a technique that mimics the downscaling of climate models, in order to test the robustness of solutions provided by the energy system model. The energy system model will constrain the capacity expansion for the power system model, while the power system model will increase temporal resolution and improve the approximation of the transmission network. With this work, we aim to support the advancement of the power infrastructure of the Southern African Power Pool (SAPP) (SAPP, 2021), which is one of the most interesting regions of the world for energy and power systems research. Indeed, driven by population growth, urbanization, and economic development, its energy systems will expand and change significantly to produce reliable and clean energy.

We assess the differences in electrical operations within the energy and power system models and examine the power generation deficit and the transmission line overloads, in order to identify their causes and to suggest potential technical solutions.

Our contribute consists of developing a new methodology for supporting long- term energy planning that evaluates the robustness and reliability of interconnected power systems under increasing electricity demands and dominated by non-dispatchable VRES. By using a power system model forced with inputs from an energy system model, we achieve a more detailed resolution than the typical energy system model, enabling us to capture the availability patterns of the variable renewable power sources and unmet demand.

5.1 Methodology

5.1.1 PowNet

PowNet is a least-cost optimization model for the simulation of the Unit Commitment (UC), i.e. when to start up or shut down power plants, and Economic Dispatch (ED), i.e. how much power should each plant generate. It is used for large- scale (regional to country) power systems modelling with an hourly time step. The power system is represented by a set of nodes that include power plants, high-voltage substations, and import/export stations (for cross-border systems) and they can transfer electricity between each other thanks to interconnections. The model looks for the least-cost scheduling and dispatch from all the power plants considered to meet hourly electricity demand in all the substations. Each node can have an associated power demand, dispatch- able power plants, renewable generators, and high-voltage substations. The model's planning horizon covers 24 hours. The objective of PowNet is to meet the hourly electricity demand at each node while minimizing the costs associated with energy generation in a planning horizon of one day. It is implemented in Python and any standard optimization solver (e.g. Gurobi, CPLEX) can be used (Chowdhury et al., 2020).

5.1.2 OSeMOSYS

OSeMOSYS, i.e., Open Source Energy MOdelling SYstem, is a dynamic, bottom-up, multi-layer freely available energy system optimization model for long-run energy planning, developed at KTH Royal Institute of Technology, Sweden. Compared to other energy system models, it needs a less significant learning curve and time effort to work, and, since it does not require any financial investment, OSeMOSYS is an accessible modelling tool for any researcher, student, or government specialist that needs to analyze an energy system (Howells et al., 2011). The reference version of OSeMOSYS, adopts the Linear Programming optimization technique and the related high-level mathematical programming language GNU Mathprog. Linear programming is a method to achieve the best outcome (such as maximum profit or lowest cost) in a mathematical model whose requirements are represented by linear relationships. Indeed, OSeMOSYS determines the optimal investment strategy and production mix of technologies and fuels required to satisfy an exogenous energy demand (Taliotis et al., 2016). The objective is to minimize an energy system's net present value (NPV) costs to meet given demands for energy carriers, energy services, or other proxies over a predefined, multi-year, horizon. The energy system is represented by a set of technologies and energy carriers. Each technology either uses and/or produces an energy carrier.

The optimization problem is solved for every slice in which the year is split. The optimization horizon includes the years between 2015 and 2070 and it produces multiple output with an yearly time step, including the total capacity for each technology.

OSeMOSYS -TEMBA is the implementation of OSeMOSYS for the African continent (The Electricity Model Base for Africa). It was first developed as a power system model (Taliotis et al., 2016) and then evolved into an energy system model. It is developed with the United Nations Economic Commission for Africa (UNECA) and the objective is to analyze the continental-scale African energy system. It covers the years between 2015 and 2070 and runs on a yearly basis, with a seasonal time step divided into night and daytime slices Each country is represented by a node, that includes the total demand of the nation and all the technologies that use or produce energy carriers. The objective of the model is to find the least cost arrangement of investment and operation system in the current situation and in the future. The nodes are connected through gas and electricity trade links, in order to satisfy the total final energy demand. Three different climate scenarios are assumed: no climate policy and constrained to 2.0 °C and 1.5°C warming constraining emissions to a consistent pathway. The Reference scenario, with no climate policy, projects the current situation into the future, where the energy policies do not evolve. Instead, in the two mitigation scenarios constrained to 1.5°C and 2.0°C there is the assumption that the African countries will need to reduce their electricity consumption by 11% and 27% respectively compared to the Reference scenario (Pappis et al., 2019).

In this work we relied on previous projections of cost-optimal hydropower expansion in the African continent (Carlino et al., 2023). These projections combine the Shared Socio Economic Pathways (SSPs) and Representative Concentration Pathways to build three scenarios harmonizing climate change impacts on water availability, climate policy assumptions, land-use change, and socioeconomic projections. The scenarios we consider are the following: SSP1-2.6, SSP4-6.0 and SSP5-8.5.

5.1.3 Methodology flowchart

To assess the robustness and the reliability of the power capacity expansion derived from the energy system model we perform a downscaling in time using the power system model forced with input derived from the energy system model. To this aim, the two models, the data processing for the power system model input are combined (Figure 15). First, we used the results of several studies to obtain hourly generation profile and the installed capacity of the variable renewable resources, then we extracted some inputs and output, namely the long-term energy projections, from OSeMOSYS-TEMBA. Finally, PowNet simulates the power system in specific years of interest, and we use the outputs to examine how different capacity expansion plans lead to specific power deficits and transmission line overloads.

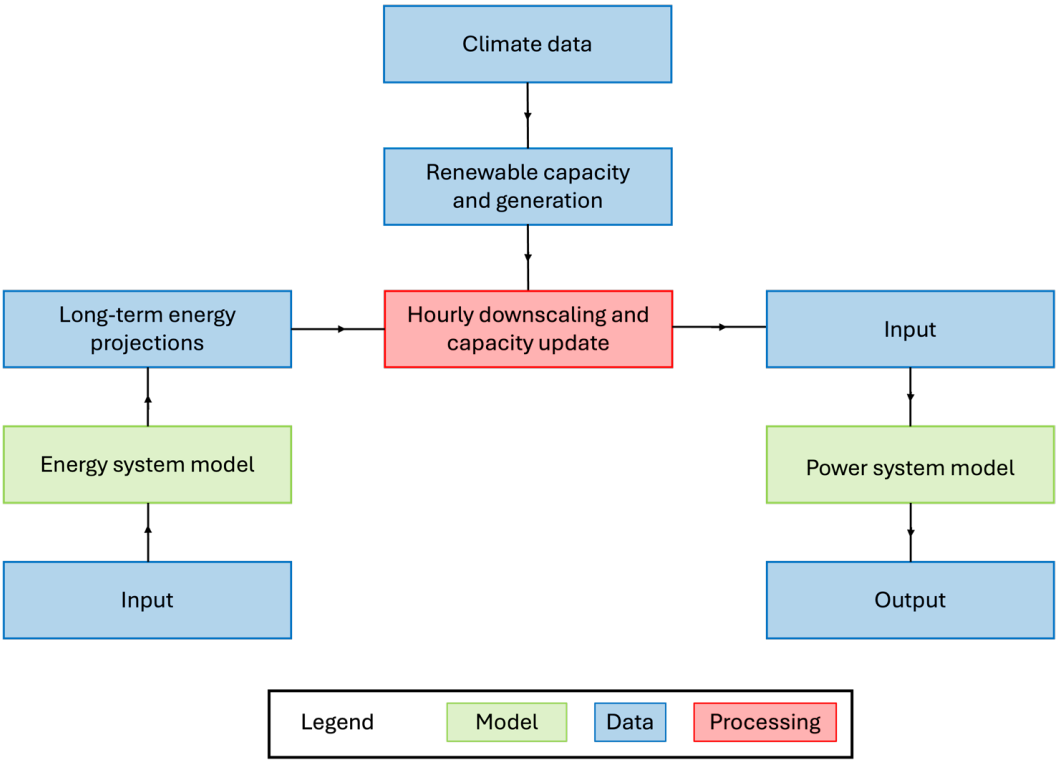

Figure 15: Flowchart of the modeling framework: both input and output of the energy system model are used, together with other datasets, to prepare input for the power system model; the power system model simulates the power system over specific years of interest.

5.1.3.1 Nodes

First, we defined the nodes in PowNet: for each country considered, one node contains the power demand and all the dispatchable units (coal, oil, gas, biomass, and nuclear) within that country. Additionally, we added one sub-node for each variable renewable resource to each country and a power deficit technology for each node *n*. The power deficit technology has a very high (ideally infinite) maximum capacity to allow the problem to find a feasible solution also when the total installed capacity is not enough to meet the demand. Yet, the variable cost of this technology is very high (ideally to represent the damage resulting from unmet demand) so the optimizer uses it as little as possible. After that, we determined the technologies that needed to be transferred from OSeMOSYS to PowNet. To do so, we chose the OSeMOSYS technologies from the "Power Plants" set and we grouped them into the following corresponding PowNet technology subsets: Biomass, Coal, Oil, Natural gas, Nuclear, Hydropower, Solar and Wind. Similarly, we considered the transmission lines of the OSeMOSYS model, i.e., the technologies belonging to the "Export electricity" set. Specifically, we used the ones connecting the countries of interest for the power system simulator.

The solar and the wind groups, unlike the dispatchable unit groups, include technologies with different patterns of availability that need to take into account. For this reason, we initially added a sub-node for each type of technology belonging to the solar or wind group to characterize their availability patterns. Subsequently, to reduce the computational effort of the PowNet model, we grouped some of these technologies together. Specifically, we did not

group technologies that can store electricity together, to assess the availability of electricity for storage and its potential usage (Figure 16).

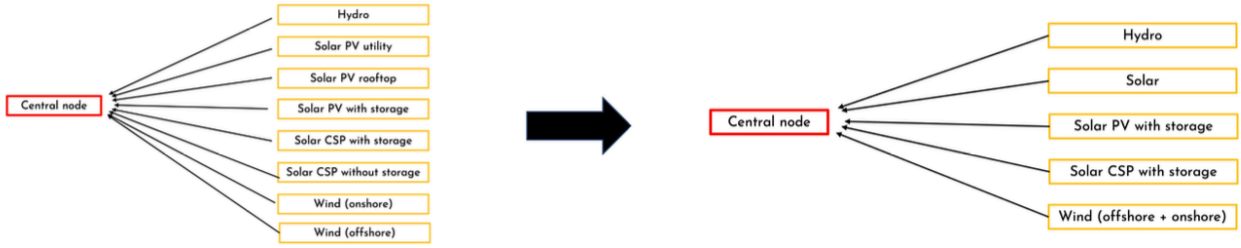

Figure 16: On the left graphical representation of central and sub-nodes in PowNet with disaggregated sub-nodes, on the right graphical representation of central and sub-nodes in PowNet with aggregated sub-nodes

5.1.3.2 Electricity demand

The second challenge was translating the electricity demand. In OSeMOSYS the electricity demand is annual, and it had to be scaled to the hourly level for PowNet. We computed the hourly electricity demand for each country ($Y_{h,n}$) by adopting a scaling factor for each hour and each country which partitions the values of annual electricity demand from OSeMOSYS, Z_n. The scaling factor is simply obtained by dividing the hourly observed electricity demand, $\bar{X}_{h,n}$, by the annual observed electricity demand, $\bar{Z}_n$. This temporal downscaling of electricity demand can be described as follows:

$$1) \quad \forall\, h, n \qquad Y_{h,n} = \bar{X}_{h,n} \cdot \frac{Z_n}{\bar{Z}_n}$$

Where *n* is the country node and *h* is the hourly time step considered.

5.1.3.3 Total installed capacity: transmission lines

The capacity of the transmission lines between nodes is obtained from the values of existing and new capacity, which are respectively an input and an output of the OSeMOSYS model. These values are summed for each transmission line (Eq. 2). It is important to underline that the residual capacity is a unique value for each year *y*, while the new capacity of a specific year is obtained by summing all the new capacities of the previous years until the considered year *y*.

For example, let us consider the situation when OSeMOSYS-TEMBA model horizon starts in 2015 for the availability of data in that year. If we have to find the total capacity of a transmission line for the year 2030, we need to sum the residual capacity of the year 2030, i.e., the existing capacity minus the retired capacity between 2015 and 2030, which is an input to the model. After that, the new capacities built from the year 2015 until 2030 need to be added to obtain the capacity existing in 2030 and to be used in PowNet to simulate the year 2030.

$$2) \quad \forall\, t, y \qquad T_{t,y} = \sum_{transline \in t} (R_{t,y} + \sum_{i=2015}^{y} N_{t,i})$$

Where $T_{t,y}$ is the final capacity, while $R_{t,y}$ and $N_{t,i}$ are the residual and the new capacity for the transmission line *t* and the considered year *y* respectively.

5.1.3.4 Total installed capacity: dispatchable units and renewable resources

For dispatchable units and renewable generators excluding hydropower, we derive the future installed capacity by adding the capacity expansion optimized by the energy system model to the presently installed capacity. In our case, the year 2022 is our baseline and data is derived from available databases and projections reporting data at the country level (Stevanato et al., 2021). We consider the operation life of each power plant in order to account for the retired capacity between the year 2022 and the year for which we are interested in producing an hourly power system simulation. Then, we group the different power technologies according to the predefined technology groups to derive the total installed capacity for each group, for each country and year considered.

Since PowNet requires a value for maximum and minimum capacity for each group of dispatchable units, we set the value of total capacity as the value of the maximum capacity (Eq. 3). We calculated the minimum capacity as a percentage of the maximum capacity (*a*), depending on the type of technology considered (Eq. 4).

$$3) \quad \forall\, g, y \qquad C_{g,y} = \sum_{tech \in g}\left(R_{g,y} + \sum_{i=2022}^{y} N_{g,i}\right)$$

$$4) \quad \forall\, g, y \qquad c_{g,y} = a \cdot \sum_{tech \in g}\left(R_{g,y} + \sum_{i=2022}^{y} N_{g,i}\right)$$

Where *C* is the maximum capacity, *c* is the minimum capacity, g is the technology considered and *a* is a value between 0 and 1.

5.1.3.5 Power generation of renewable resources

The renewable resources, excluding hydro technology, include solar PV rooftop, solar PV utility, solar PV with storage, solar CSP with and without storage, onshore wind, and offshore wind. We obtained hourly generation profile for these technologies from available datasets. To meet PowNet's requirement of aggregating power plants of the same category located within the same country into a single node, we assume that all sub-nodes are located in the geometric centre of their respective countries. Afterwards, to reduce the computational time of the PowNet's simulations, as mentioned earlier, we aggregated the wind offshore and the wind onshore technologies into the "wind" sub-node, and the solar PV rooftop, the solar PV utility and the solar CSP without storage technologies into the "solar" sub-node (Figure 16). As a result, each country is represented by one central node containing dispatchable units, deficit and load, along with five sub-nodes: Wind, Solar, Solar PV with storage, Solar CSP with storage and Hydro. The renewable resources with storage are not combined with other technologies, allowing for the management of stored electricity when available. The power generation of the hydro power technology *HG* for each country *n* is instead obtained summing the generation from each hydro power plant located within the that country. The power generation is computed multiplying the installed capacity *C* and the monthly capacity factors *MCF* of each hydro power plant *hp* located in the considered countries (Eq. 5).

5) $\forall\, n, h \qquad HG_{n,h} = \sum_{hydropowerplant \in hp}(C_{hp} \cdot MCF_{hp}) \cdot 1h$

5.1.4 Case study

5.1.4.1 Southern African Power Pool

The Southern African Power Pool (SAPP) is a region that includes twelve countries, namely, Angola, Botswana, the Democratic Republic of the Congo, Lesotho, Malawi, Mozambique, Namibia, South Africa, Swaziland, Tanzania, Zambia, and Zimbabwe. At present, coal generation constitutes the majority share of the SAPP's generation mix, accounting for 59%. In addition to coal (thermal), in SAPP other generation technologies are available, including hydropower, solar, distillate fuel oil, nuclear, wind, gas, biomass, and landfill or waste. The total installed generation capacity in the 12 countries is 80 923 MW with an operating capacity of 65 198 MW and a demand and reserve of 55 235 MW, and an excess generation capacity of 9 963 MW (SAPP, 2021). Despite being the most developed regional power pool in the continent, Southern Africa's electricity trade is heavily constrained by the limitations of the transmission network. At the same time, the population is expected to grow to more than 500 million people in the next 25 years and, as a result, energy demand will increase dramatically (Spalding-Fecher et al., 2017). The SAPP region will therefore have to face two major challenges: meeting the increasing energy demand and limiting greenhouse gas emissions and their socio-environmental effects (Chowdhury et al., 2022). As SAPP moves towards cleaner sources of energy, there is a need to evaluate the reliability of the transitioning power system. Unmet demand and outages don't have to be affected by the transition to clean energy. Better than that, these events should be come less frequent to improve economic development and living standards in the member countries.

5.1.4.2 Data

To assess the differences in electrical operations within the energy and power system models and examine the electricity generation deficit and transmission line overloads we combined data from four main datasets. First, we relied on previous projections of cost-optimal hydropower expansion in the African continent computed with OSeMOSYS-TEMBA (Carlino et al., 2023), to obtain data of residual capacity and new capacity for the technologies considered and the transmission lines. Second, we used available databases and projections reporting data at the country level of installed capacity in 2022 and hourly observed electricity demand (Stevanato et al., 2021). Third, we relied on the African Hydropower Atlas (Sterl et al., 2022), to obtain the power generation from each hydro power plant within the SAPP region. Fourth, we used available datasets (Pfenninger and Staffell, 2016) to obtain hourly generation profiles for wind and solar technologies. These datasets are combined in order to prepare the inputs required by PowNet, that is implemented in this work, at the SAPP level. The optimization horizon is of 1 year with an hourly time step. The twelve countries that comprises the SAPP region can transfer electricity between each other thanks to interconnections. PowNet represents the power system with a set of nodes, and they can exchange electricity using a power grid. A node can represent in a specific country the set of dispatchable units, the set of technologies that produce solar power, set of technologies that

produce solar PV with storage, set of technologies that produce solar CSP with storage, the set of technologies that produce hydropower, and the set of technologies that produce wind power. From OSeMOSYS-TEMBA we choose the technologies that have to be transferred in PowNet, and they belong to the "Power plants" sets. In each demand node, the power-generating technologies are grouped into the following PowNet subsets:

- Biomass: Biomass & Waste CHP plant with CCS - Air cooling, - MDT cooling, - NDT cooling, - OTF/OTS cooling, Biomass & Waste CHP plant - Air cooling, - MDT cooling, - NDT cooling, - OTF/OTS cooling.
- Coal: Coal power plant with CCS - Air cooling, - MDT cooling, - NDT cooling, - OTF/OTS cooling, Coal power plant - Air cooling, - MDT cooling, - NDT cooling, - OTF/OTS cooling.
- Oil: Oil-fired gas turbine (SCGT) - Air cooling (old), - MDT cooling (old), - NDT cooling (old), - OTF/OTS cooling (old), Oil-fired gas turbine (SCGT) - Air cooling (new), - MDT cooling (new), - NDT cooling (new), - OTF/OTS cooling (new), Light Fuel Oil stand-alone (1kW), Light Fuel Oil power plant - Air cooling (old), - MDT cooling (old), - NDT cooling (old), - OTF/OTS cooling (old), Light Fuel Oil power plant - Air cooling (new), - MDT cooling (new), - NDT cooling (new), - OTF/OTS cooling (new).
- Natural gas: Natural gas power plant (combined cycle) - CCS - Air cooling (new), - MDT cooling (new), - NDT cooling (new), - OTF/OTS cooling (new), Natural gas power plant (combined cycle) - Air cooling (old), - MDT cooling (old), - NDT cooling (old), - OTF/OTS cooling (old), Natural gas power plant (single cycle) - CCS - Air cooling (new), - MDT cooling (new), - NDT cooling (new), - OTF/OTS cooling (new), Natural gas power plant (single cycle) - Air cooling (old), - MDT cooling (old), - NDT cooling (old), - OTF/OTS cooling (old).
- Nuclear: Nuclear power plant - OTS/OTF cooling (old), Nuclear power plant - OTS/OTF cooling (new)
- Hydropower: hydropower plants within SAPP.
- Solar: CSP (without storage), solar PV (utility), solar PV (rooftop).
- Solar PV with storage: solar PV with storage
- Solar CSP with storage: CSP (with storage)
- Wind: wind (onshore), wind (offshore).

where CHP stays for Combined Heat and Power, CCS for Carbon Capture and Storage, SCGT for Simple Cycle Gas turbine, and CSP for Concentrating Solar Power. Addition- ally, the following cooling technologies are reported with acronyms: MDT for Mechanical Draft Tower, NDT for Natural Draft Tower, OTF for Once Through Freshwater, and OTS for Once Through Salt water.

The PowNet's inputs that are not taken from OSeMOSYS-TEMBA, are the following ones:

- TransLoss, that is the parameter used to discount the energy production by a given percentage, and in our case is equal 0.075 (Chowdhury et al., 2020).

- N1criterion, that is a parameter that leaves the part of the transmission lines' capacity unused, allowing for any hypothetical reactive power flows, and in our case is equal to 0.85
- ResMargin, that is the percentage of the system's demand used in the electricity reserve constraint, and in our case is equal to 0.15 (Chowdhury et al., 2020).
- SpinMargin, that is the percentage of the total reserve, used in the electricity reserve constraint, and in our case is equal to 0.5 (Chowdhury et al., 2020).
- Fixed O&M costs, variable O&M costs for each type of technology (Tidball et al., 2010).
- Fuels price (IEA-ETSAP, 2010).
- Start-up costs, ramp, minup time mindown time, heat rate of each technology and fuel price (Chowdhury et al., 2020, (Hörsch et al., 2018)
- DerateF used to account for the impact of droughts on freshwater- dependent dispatchable units, and in our case is assumed ideal, which means equal to 1. This reflects the assumptions that cooling system are always able to work and power plant efficiency is not affected at any time step by water scarcity.
- The values of the parameter *a,* which is used to compute the minimum capacity of the dispatchable units (("Innovation landscape brief: Flexibility in conventional power plants," n.d.).

5.2 Numerical Results

Three main simulations are conducted in year 2030, using a combination of the Shared Socioeconomic Pathways (SSPs) and Representative Concentration Pathways, namely SSP1-2.6, SSP4-6.0, and SSP5-8.5. SSP1-2.6 scenario aims to maintain the global mean temperature below 2°C, while SSP4-6.0 and SSP5-8.5 scenarios are characterized by higher levels of warming and by rising inequalities and fossil-fueled development, respectively.

5.2.1 Power generation mix, deficit and violation of the transmission lines analysis

In all the simulations computed with PowNet, the percentage of power generation particularly from coal, but also from gas, nuclear and solar in the annual generation mix increases compared to OSeMOSYS-TEMBA. This difference is compensated by the decreased use of wind and hydro power. This trend can be attributed to the significant concentration in PowNet of hydropower generation available within the Democratic Republic of Congo. However, the existing transmission lines do not possess sufficient capacity to facilitate the transfer of the entire available hydropower generation, resulting in a decrease in hydro generation for these scenarios.

In addition, all three simulations show a percentage of deficit, indicating that the power generated is insufficient to meet the demand. In the last two scenarios, the percentage of deficit increases compared to the reference scenario mainly as a result of reduced coal use and insufficient power generation. The peak of the mean hourly probability of power generation deficit is located between 7 and 9 pm, therefore in the evening and the countries

with the highest deficit are Zambia and Tanzania in all three simulations, but it is also noticeable in Angola and in the SSP1-2.6 scenario in Malawi (Figure 17).
The peak of the mean hourly probability of violation of the transmission lines is also located during the evening. The transmission lines with a percentage of violation higher than 75% are mainly the ones connecting the Democratic Republic of Congo with Zambia and Angola (Figure 18). This situation can be attributed to the abundant hydroelectric power generation capacity in the Democratic Republic of Congo, primarily attributable to the presence of the Inga 3 hydropower plant, boasting a remarkable capacity of 11050 MW. Nonetheless, there are other transmission lines with a percentage of violation higher than 40% connecting other countries experiencing power generation deficit.

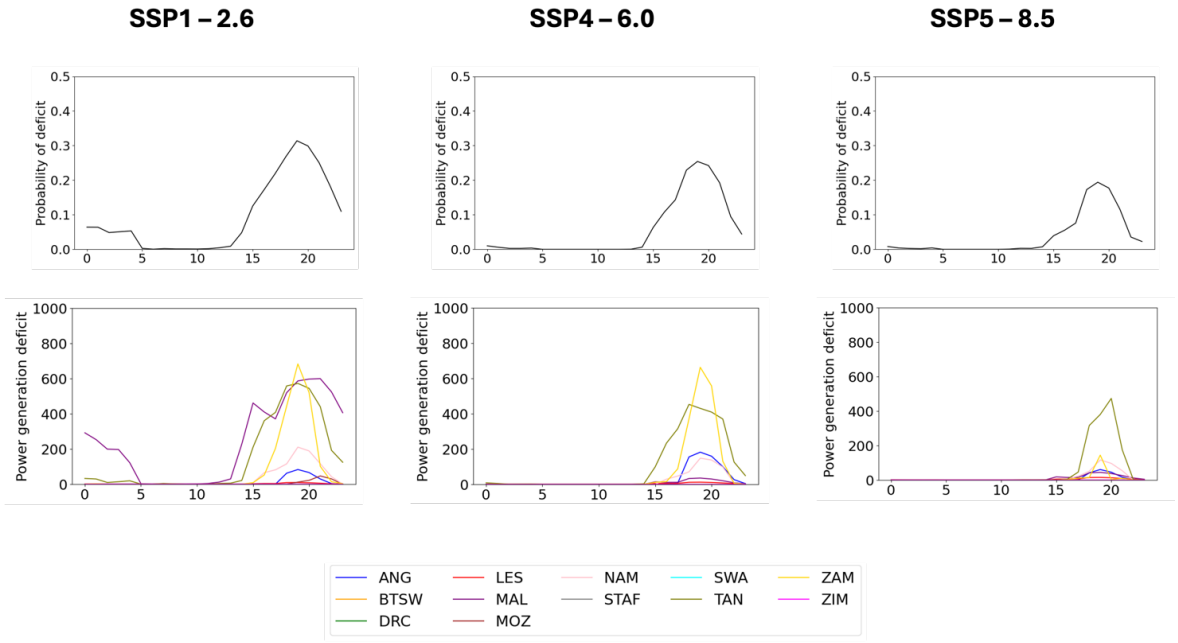

Figure 17: Mean hourly probability of deficit.

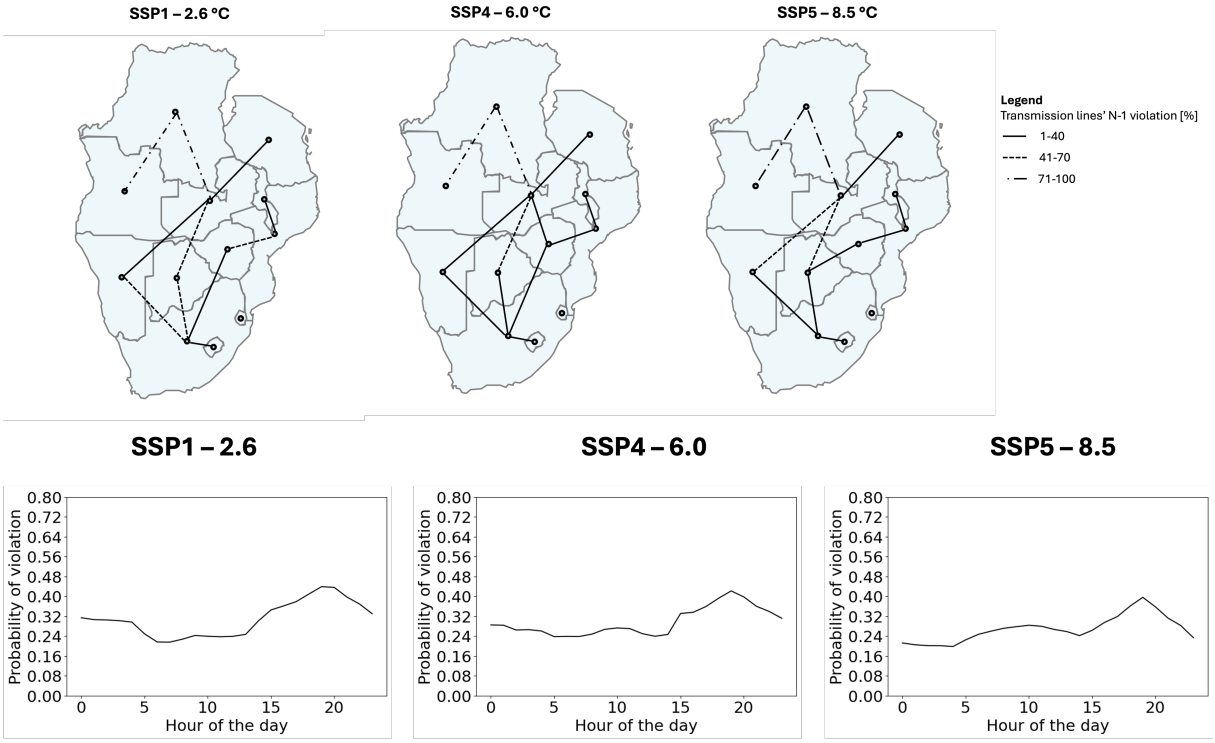

Figure 18: Analysis of the transmission lines. The maps report the transmission lines with an annual percentage of violation higher than 0, while the plots report the mean hourly probability of violation of the transmission lines.

5.2.2 Peak power demand analysis

To understand the causes behind the occurrence of the power generation deficit, we focused on the hour of maximum power demand, which is 9 pm on October 30th, 2030 for the scenarios SSP1-2.6 and SSP4-6.0 and 9 pm on October 31st, 2030 for the scenario SPP5-8.5. The bars in Figure 19 represent the average power output of OSeMOSYS-TEMBA, which is the annual generation mix divided by the number of hours in a year (8760), and the power output of PowNet in the hour of peak power demand. The power generation during this hour is unable to meet the demand, resulting in a deficit in the PowNet peak power output bar. In all the scenarios, OSeMOSYS-TEMBA is planning the capacity expansion based on average power demand, resulting in insufficient available capacity to meet the peak demand observed at the hourly resolution in PowNet.

The deficit in the hour of peak demand arises in all the scenarios from the lack of installed capacity in the countries where the deficit occurs and from the fact that transmission lines connecting these countries with others are already used at maximum capacity (Figure 20 , Figure 21, and Figure 22). In the SSP1-2.6 and SSP4-6.0 scenarios (Figure 20 and Figure 21) the deficit is particularly high in Malawi, Zambia and Tanzania, but also in Namibia and Angola, and it cannot be reduced with the existing transmission lines, which are almost fully saturated. Increasing the installed capacity is necessary to reduce the deficit. However, increasing the capacity of transmission lines between Zambia, Angola and Democratic Republic of Congo could reduce the shortfall. In the SSP5-8.5 scenario (Figure 9) the deficit is

mostly concentrated in Tanzania and Namibia, where the total installed capacity must increase to meet their electricity demand.

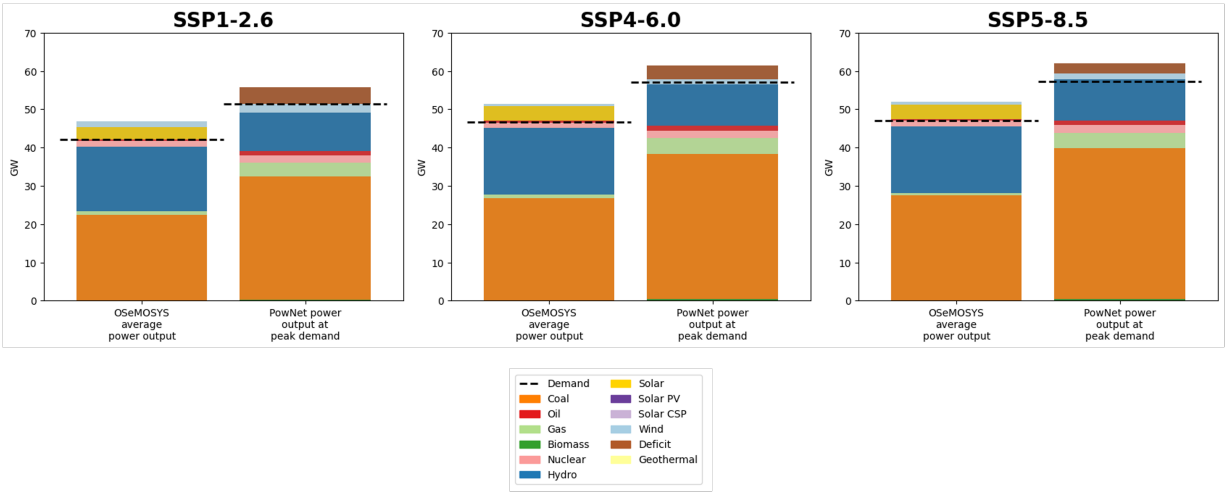

Figure 19: Peak power demand analysis. OSeMOSYS-TEMBA's average generation mix and PowNet's generation mix in the hour of peak power demand.

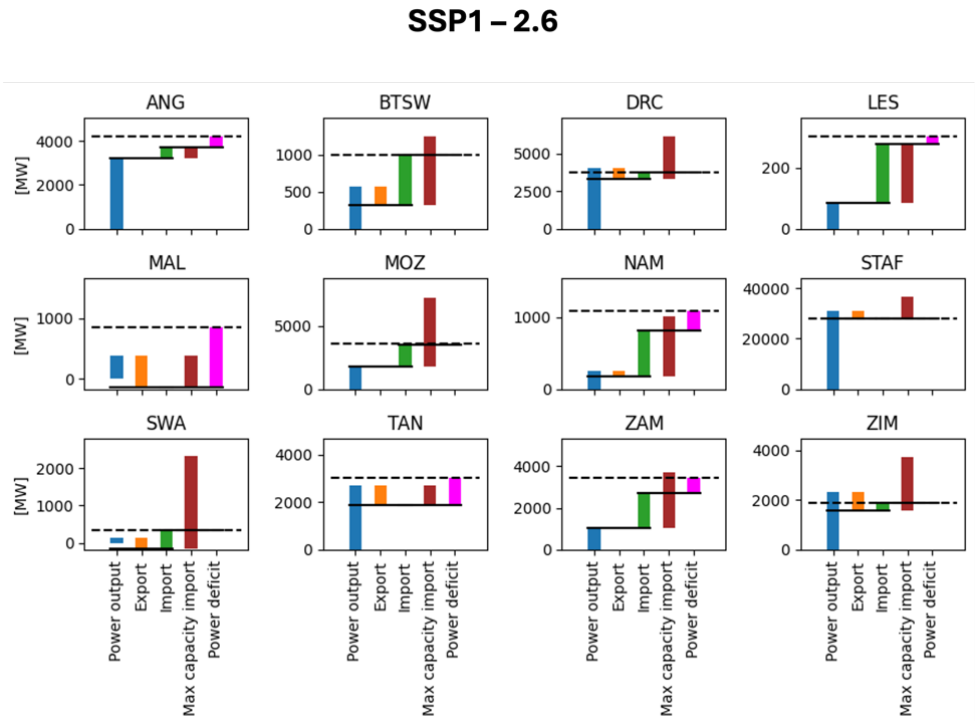

Figure 20: Power flow analysis during the hour of peak demand with scenario SSP1-2.6

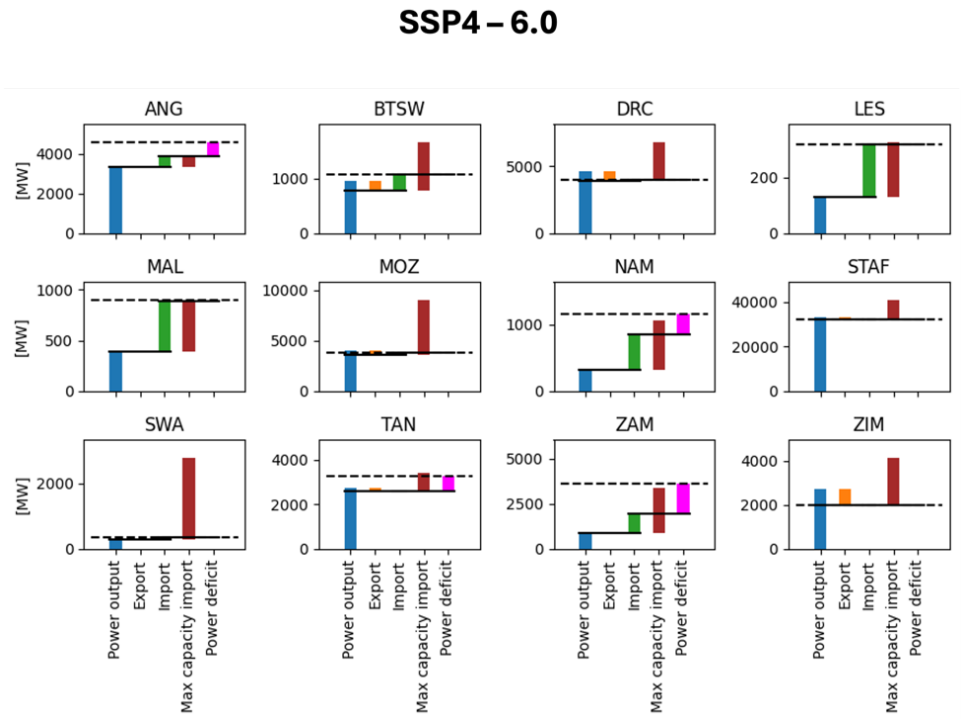

Figure 21: Power flow analysis during the hour of peak demand with scenario SSP4-6.0

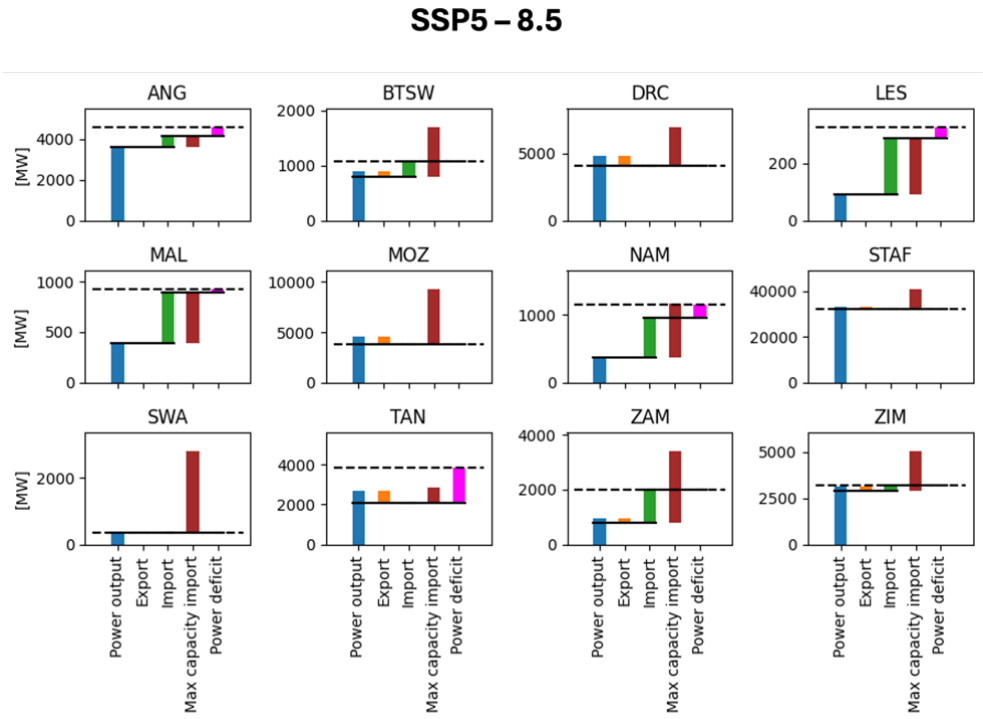

Figure 22: Power flow analysis during the hour of peak demand with scenario SSP5-8.5.

5.2.3 Hydropower potential

In the Democratic Republic of the Congo and, to some extent, in Angola, the hydropower generation that is actually integrated into the grid is significantly lower in all the scenarios

when compared to the total hydropower generation available (Figure 23). To potentially reduce the power deficit, a feasible solution would be to store unused water for future power generation within the available reservoirs. This stored water could then be exploited during periods of high demand. The Democratic Republic of Congo has the capacity to store a substantial volume of water, approximately 2985.465 million cubic meters without considering the dead volume, which translates to a potential hydropower generation of 534.6208 GWh. Meanwhile, Angola has the capability to store around 8319.864 million cubic meters of water, corresponding to a hydropower generation potential of 2449.05 GWh. However, in order to exploit this hydropower potential, additional capacity needs to be installed for all the scenarios in the transmission lines between the Democratic Republic of Congo and Zambia, as well as between the Democratic Republic of Congo and Angola, as they are already operating near their maximum capacity. The power deficit, as stated before, has peak during the evening, around 7 pm. Furthermore, the power deficit is more pronounced during the months from July to October when the available hydropower generation is at its lowest. However, by storing unused water primarily in the Democratic Republic of Congo and secondarily in Angola, it is possible to mitigate this deficit.

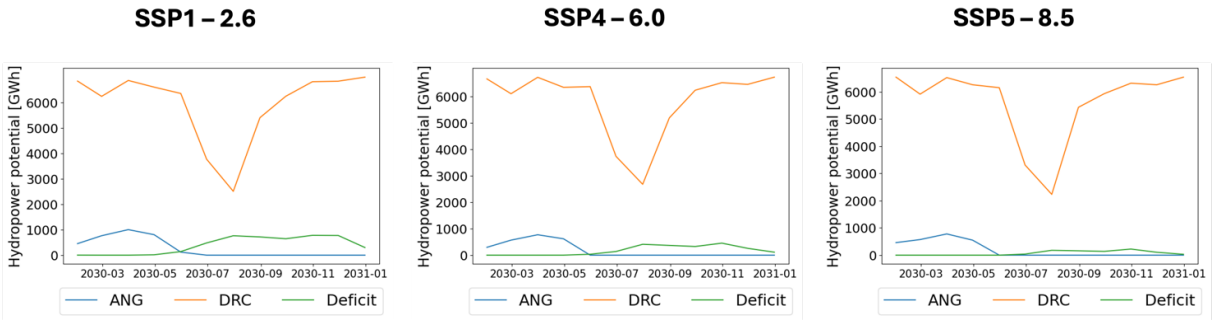

Figure 23: Hydropower potential and power deficit.

6 Including local crop production functions in large-scale agricultural models

The reasons why this feedback loop is relevant have been acknowledged and stated in CAPRI's development to better account for food-water linkages (Blanco et al., 2018). One of the main improvements indicated was the improvement on water availability and abstraction modelling. This improvement has been addressed in GoNEXUS through an interconnection between CAPRI and PCR-GLOBWB2 at the global level and between CAPRI and LISFLOOD at the EU level (more details inD3.2). The feedback loop previously described on improving operating rules could also result into an improvement on CAPRI. The implementation of a feedback loop between a local hydrological or water resource management model and CAPRI would be solved the same way as the linkage between CAPRI and PCR-GLOBWB2/LISFLOOD described in D3.2.

The inclusion of local crop production functions in CAPRI would enable a more precise assessment of irrigation needs and the impact of irrigation deficits on crop productions, which depend on the local soil and irrigation practices. The methodology proposed, combining FAO56 (Allen et al, 1998) and FAO66 (Steduto et al., 2012), would also address in an efficient manner the intra-annual climatic patterns, as well as how they interact with the local irrigation practices, by adopting a daily scale in its building. The implementation of such a feedback loop directly into CAPRI formulation would be infeasible due to the associated computational burden, as acknowledged in Blanco et al (2018), but the off-line calculation of production functions would enable their efficient and sequentially uptake. This feedback loop is presented in a theoretical way in order to describe how these curves would be derived.

6.1 Methodology

The methodology followed for the elicitation of production curves can be divided into the main type of crop considered: fruit trees and annual crops.

6.1.1 Production curves for fruit trees

The calculation of the production curves for fruit trees follows, on a broader view, the FAO Irrigation and Drainage Paper 33 (Doorenbos et al., 1979) and the FAO Irrigation and Drainage Paper 66 (Steduto et al., 2012). These reports establish a relationship between crop evapotranspiration and crop yield, which can be directly translated into scarcity costs by multiplying it by the crop price. This approach is the one already considered by CAPRI in rainfed and irrigated agriculture (Blanco et al, 2018).

However, in this feedback loop crop evapotranspirations (ETc) for the fruit trees present in the Jucar river basin were calculated applying a soil balance at the daily scale including the current irrigation practices.

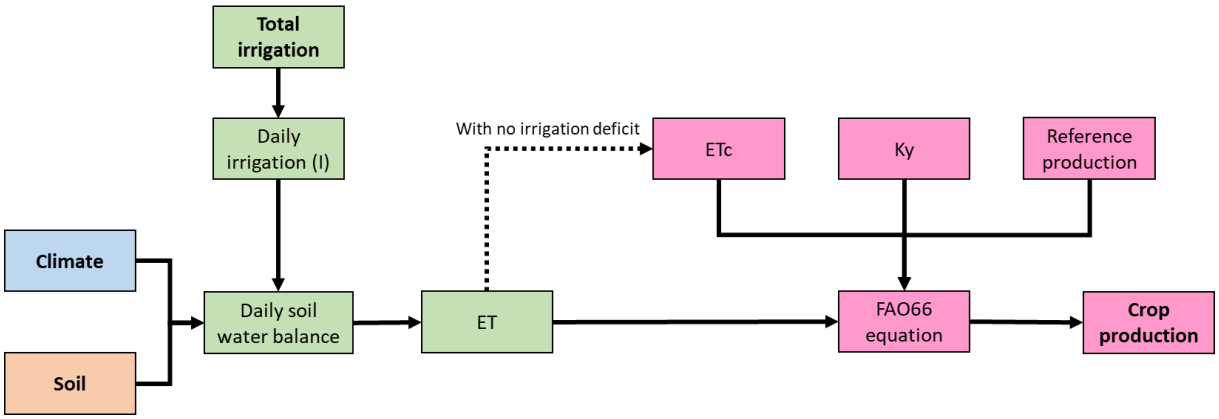

Figure 24: Flowchart used to compute crop productions

For each fruit tree, the procedure described in the FAO Irrigation and drainage paper 56 (FAO 56, Allen et al, 1998) was followed, calculating the reference evapotranspiration ETo and then applying the corresponding crop coefficient Kc to transform ETo into ETc. ETc values for each year and fruit tree were computed based on the climatological data provided by the CMIP6 scenarios considered in GoNEXUS (see deliverables D2.1 and D2.2), the soil features and the crop yield coefficient (ky) and reference production or yield. Reference productions for the fruit trees of the Jucar river basin were obtained the annual statistics published by the Ministry for Agriculture, Fishery and Food of Spain or from the Survey on Crop Surface and Production of Spain (ESYRCE). To derive each production function, a set of total irrigation levels were used as input and downscaled into daily irrigation levels (I). Then, the daily water balance and daily ET (E+Tr) values were computed and aggregated at the annual scale (next equation and Figure 25). The adoption of the daily scale is crucial in this regard to account for the soil water balance and water uptake from crops, as well as to account for the features of the irrigation practices used in the area.

$$W_{r,t+1} = W_{r,t} + (P - RO) + I + CR - E - Tr - DP$$

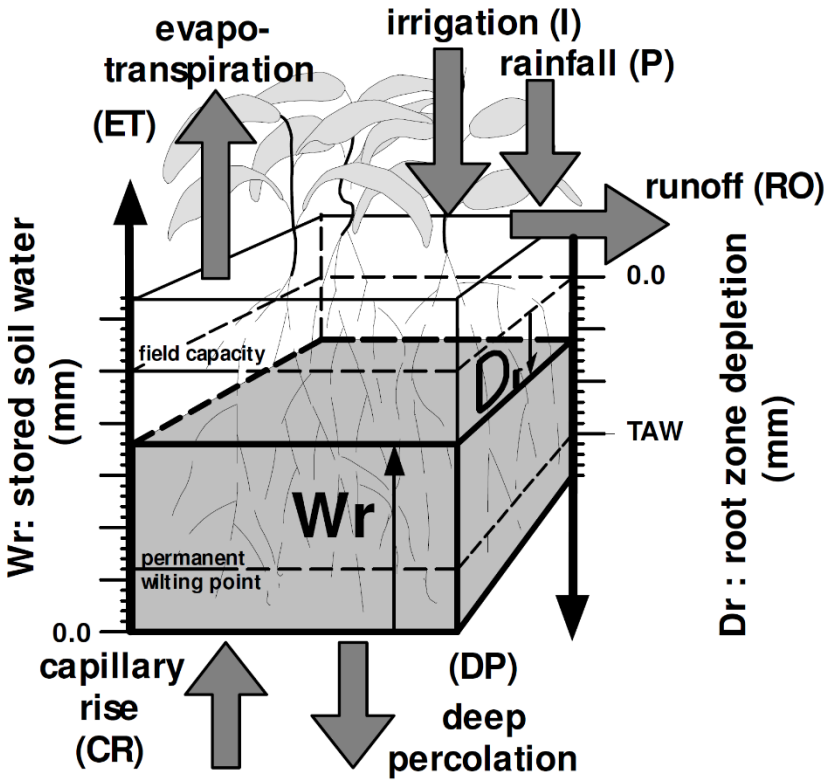

Figure 25: Soil water stocks and flows considered by FAO56 (FAO, 2023)

6.1.2 Production curves for cereals

Crop production and water needs for cereals have been calculated using the AquaCrop-OSPy tool (https://pypi.org/project/aquacrop/), which fits in an adequate way the features of annual crops. AquaCrop-OSPy follows FAO 56, FAO33 and FAO 66 processes, as well as for the case of fruit crops. The only difference refers to the yield calculations, which in Aquacrop are expressed in terms of biomass (B) and harvest index (HI), in which yield is defined as the product between them. Figure 26 summarizes the stocks and fluxes considered by Aquacrop.

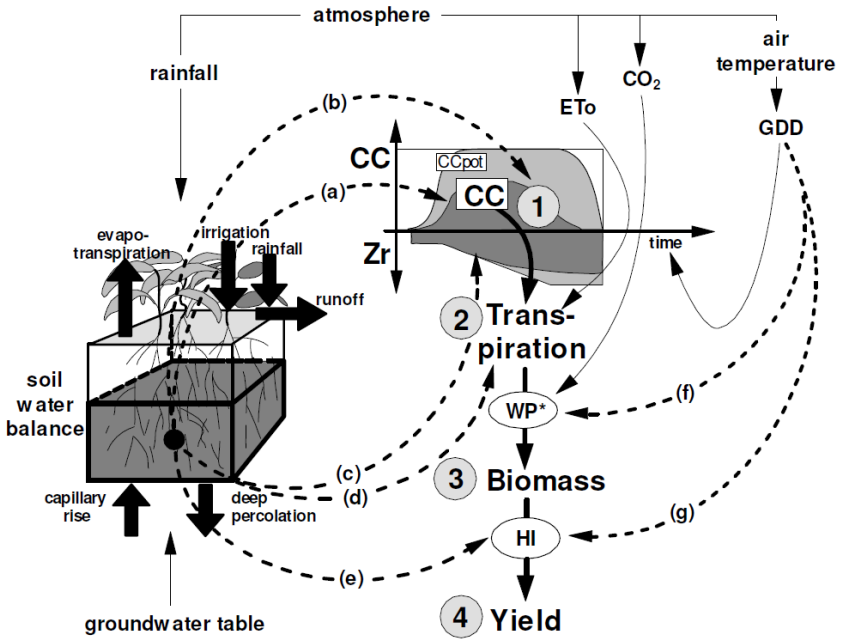

Figure 26: Stocks and fluxes considered by Aquacrop-OSPy (FAO, 2023)

6.2 Numerical Results

The results obtained are production functions per type of crop and year, tailored to the particular features of climate (at the daily scale) and soil of the Jucar river basin. Those express the relationship between water applied and crop yield per year. Some of them are shown as example below.

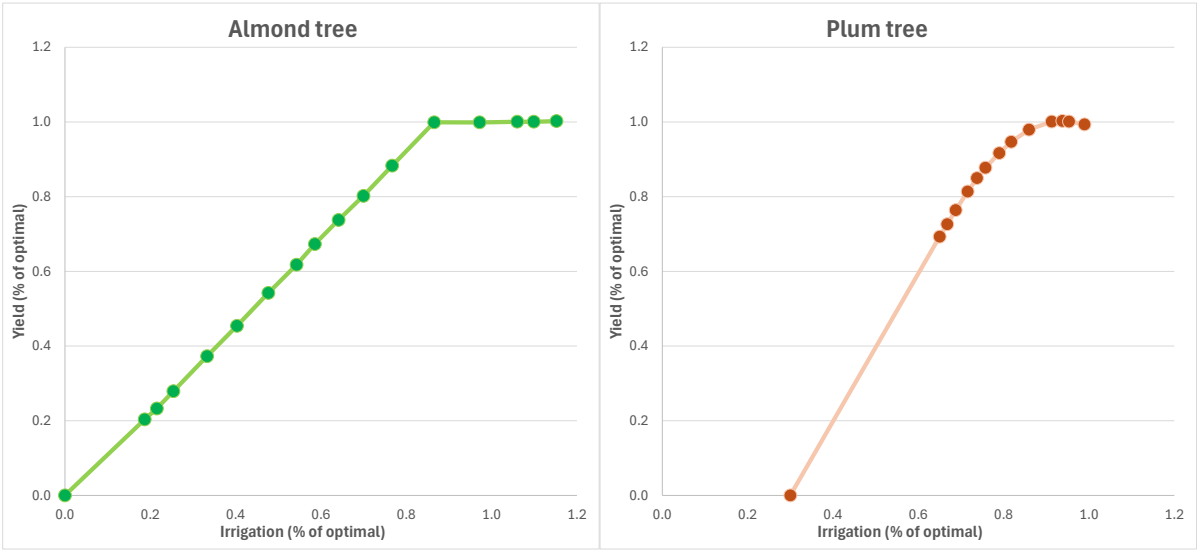

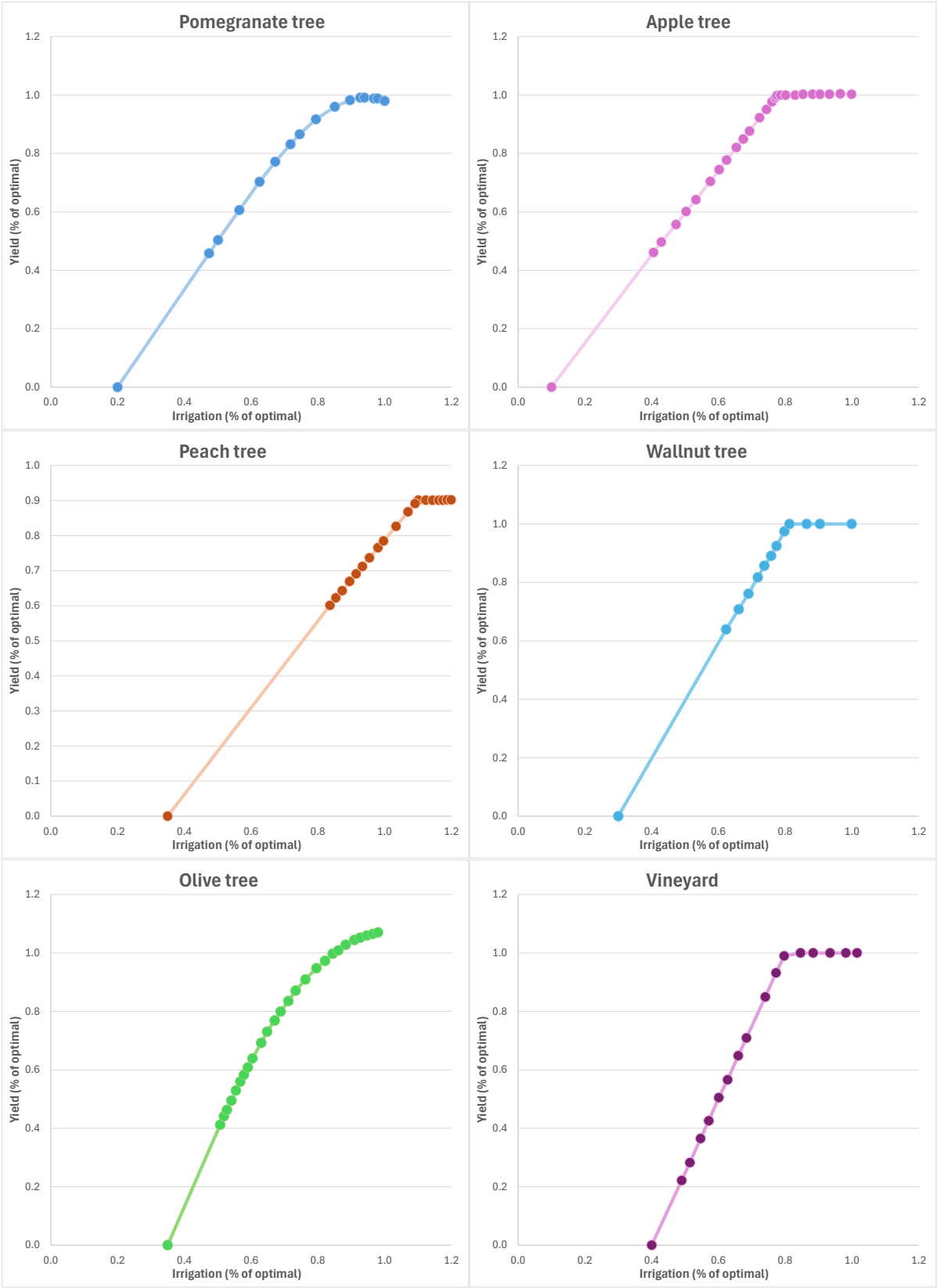
Pomegranate tree
Yield (% of optimal)
Irrigation (% of optimal)
Apple tree
Yield (% of optimal)
Irrigation (% of optimal)
Peach tree
Yield (% of optimal)
Irrigation (% of optimal)
Wallnut tree
Yield (% of optimal)
Irrigation (% of optimal)
Olive tree
Yield (% of optimal)
Irrigation (% of optimal)
Vineyard
Yield (% of optimal)
Irrigation (% of optimal)

7 Synthesis and conclusions

This document synthesizes the main findings of Task T4.6 (Feedbacks to the Global Scale), focusing on the disparities between global and local Water-Energy-Food-Ecosystem models. The analysis covers various feedback mechanisms involving selected GONEXUS case studies across different spatial scales.

Chapter 2 demonstrates that the FRB system developed for the Jucar river system performs well with a simple experimental setup, reinforcing the potential of fuzzy logic for deriving effective operating rules for complex multi-reservoir systems in global hydrologic models.

Chapter 3 reveals that water availability significantly limits hydropower generation, with 64% of modeled plants showing an average capacity factor in normal conditions below the nominal value used in continental energy systems models OsEMOSYS-TEMBA. The capacity factors are also sensitive to intra-annual, inter-annual, and climate change induced hydrologic variability, highlighting the strong limitations of assuming a homogeneous capacity factor.

Chapter 4 investigates the potential impacts of national socio-political instability on energy transition strategies in Africa as simulated by the continental energy systems models OsEMOSYS-TEMBA. The analysis identifies key risk hotspots and factors influencing energy security under various future scenarios. Despite some limitations, such as the posterior quantification of political risk and the constrained scenario assumptions, the study underscores the importance of incorporating socio-political considerations into energy system planning to ensure robust and adaptable transition strategies.

Chapter 5 shows how refining power system models to higher spatial and temporal resolutions can reveal potential vulnerabilities in long-term, continental scale energy planning projections. The integration of renewable resources requires high-frequency power operation adjustments, and existing infrastructure may not fully meet future demand. The study highlights the need for additional power generation capacity and expanded transmission infrastructure, particularly in regions like Zambia, to mitigate power shortages and enhance system reliability.

Chapter 6 describes a methodology to enhance the CAPRI agricultural model by integrating local crop production functions. This involves creating production curves that depict the relationship between water applied (irrigation) and crop yield, considering local soil and irrigation practices. The methodology differs for fruit trees and annual crops (e.g., cereals, vegetables). For fruit trees, crop evapotranspiration (ETc) is calculated using a daily soil balance, factoring in existing irrigation methods, and then linked to crop yield based on FAO guidelines. For annual crops, the AquaCrop-OSPy tool is utilized, which models water flow and crop growth to estimate yield. The resulting production functions, specific to each crop type and year, are intended to enable a more precise evaluation of irrigation needs and the impact of water scarcity within the CAPRI model.

In summary, these findings emphasize the complex interplay between global policies and local multisector dynamics. It demonstrates that global WEFE policies can have significant local ramifications and stresses the necessity of tailoring global policies to local contexts. By identifying risk hotspots and potential gaps across models, this report provides valuable insights for producing better WEFE evidence navigating the trade-off between targeting realism at the local scale and representing global socio-economic and climatic teleconnections.

8 References

ACLED, n.d. Data for Africa.

Africa Energy Outlook 2022, n.d.

Ajayi, O.O., 2013. Sustainable energy development and environmental protection: Implication for selected states in West Africa. Renew. Sustain. Energy Rev. 26, 532–539. https://doi.org/10.1016/j.rser.2013.06.009

Alushula, P., 2023. Kenya Power Turns to Detectives as Vandalism Cases Stubborn. Bus. Dly. Afr.

Andrijevic, M., Crespo Cuaresma, J., Muttarak, R., Schleussner, C.-F., 2019. Governance in socioeconomic pathways and its role for future adaptive capacity. Nat. Sustain. 3, 35–41. https://doi.org/10.1038/s41893-019-0405-0

Bai, Dr.V.R., Tamjis, Prof.M.R., 1970. Fuzzy Logic Model on Operation and Control of Hydro-Power Dams in Malaysia. Int. Conf. Comput. Exp. Eng. Sci. 4, 31–40. https://doi.org/10.3970/icces.2007.004.031

Barnes, T., Shivakumar, A., Brinkerink, M., Niet, T., 2022. OSeMOSYS Global, an open-source, open data global electricity system model generator. Sci. Data 9, 623. https://doi.org/10.1038/s41597-022-01737-0

Bauer, N., others, 2017. Shared Socio-Economic Pathways of the Energy Sector – Quantifying the Narratives. Glob. Environ. Change 42, 316–330.

Blanco, M., Witzke, P., Barreiro Hurle, J., Martinez, P., Salputra, G., Hristov, J., 2018. CAPRI water 2.0: an upgraded and updated CAPRI water module. European Commission. Joint Research Centre., LU.

Carlino, A., De Vita, A., Giuliani, M., Zamberletti, P., Capros, P., Recanati, F., Kannavou, M., Castelletti, A., 2021. Hydroclimatic change challenges the EU planned transition to a carbon neutral electricity system. Environ. Res. Lett. 16, 104011. https://doi.org/10.1088/1748-9326/ac243f

Carlino, A., Wildemeersch, M., Chawanda, C.J., Giuliani, M., Sterl, S., Thiery, W., Van Griensven, A., Castelletti, A., 2023. Declining cost of renewables and climate change curb the need for African hydropower expansion. Science 381, eadf5848. https://doi.org/10.1126/science.adf5848

CDP, 2020. Africa Report 2020 – Benchmarking progress towards climate safe cities, states, and regions.

Cherp, A., Jewell, J., Vinichenko, V., Bauer, N., De Cian, E., 2016. Global energy security under different climate policies, GDP growth rates and fossil resource availabilities. Clim. Change 136, 83–94. https://doi.org/10.1007/s10584-013-0950-x

Chowdhury, A.F.M.K., Deshmukh, R., Wu, G.C., Uppal, A., Mileva, A., Curry, T., Armstrong, L., Galelli, S., Ndhlukula, K., 2022. Enabling a low-carbon electricity system for Southern Africa. Joule 6, 1826–1844. https://doi.org/10.1016/j.joule.2022.06.030

Chowdhury, A.F.M.K., Kern, J., Dang, T.D., Galelli, S., 2020. PowNet: A Network-Constrained Unit Commitment/Economic Dispatch Model for Large-Scale Power Systems Analysis. J. Open Res. Softw. 8, 5. https://doi.org/10.5334/jors.302

Clarke, L., others, 2022. Energy Systems. In IPCC, 2022: Climate Change 2022: Mitigation of Climate Change. Contribution of Working Group III to the Sixth Assessment Report of the Intergovernmental Panel on Climate Change. Cambridge University Press, Cambridge, UK and New York, NY, USA.

Dalla Longa, F., Van Der Zwaan, B., 2021. Heart of light: an assessment of enhanced electricity access in Africa. Renew. Sustain. Energy Rev. 136, 110399. https://doi.org/10.1016/j.rser.2020.110399
Darkness Imminent as Vandals Down Transmission Lines in Fresh Attacks, 2024. . Guard. Niger.
Doorenbos, J., Kassam, A.H., Bentvelsen, C.L.M., Branscheid, V., Plusjé, J.M.G.A., Smith, M., Uittenbogaard, G.O., van der Wal, H.K., 1979. FAO Irrigation and Drainage Paper 33: Yield response to water.
ECA, 2009. The Potential of Regional Power Sector Integration, Cahora Bassa | Generation Case Study.
EIAD, n.d. Tracking Energy Attacks.
Ekel, P., Parreiras, R., Pedrycz, W., 2010. Fuzzy Multicriteria Decision-Making: Models, Methods and Applications | Wiley. Wiley.
European Commission. Joint Research Centre., 2019. Energy projections for African countries. Publications Office, LU.
FAO, 2023. Book I. Understanding AquaCrop. FAO.
Freeman, R., 2021. Modelling the Socio-Political Feasibility of Energy Transition with System Dynamics. Environ. Innov. Soc. Transit. 40, 486–500.
Frieler, K., others, 2017. Assessing the Impacts of 1.5 C Global Warming–Simulation Protocol of the Inter-Sectoral Impact Model Intercomparison Project (ISIMIP2b). Geosci. Model Dev. 10, 4321–4345.
Gold, D.F., Reed, P.M., Trindade, B.C., Characklis, G.W., 2019. Identifying Actionable Compromises: Navigating Multi-City Robustness Conflicts to Discover Cooperative Safe Operating Spaces for Regional Water Supply Portfolios. Water Resour. Res. 55, 9024–9050. https://doi.org/10.1029/2019WR025462
Hanna, R., Gross, R., 2021. How Do Energy Systems Model and Scenario Studies Explicitly Represent Socio-Economic, Political and Technological Disruption and Discontinuity? Implications for Policy and Practitioners. Energy Policy 149, 111984.
Hörsch, J., Hofmann, F., Schlachtberger, D., Brown, T., 2018. PyPSA-Eur: An open optimisation model of the European transmission system. Energy Strategy Rev. 22, 207–215. https://doi.org/10.1016/j.esr.2018.08.012
Howells, M., Rogner, H., Strachan, N., Heaps, C., Huntington, H., Kypreos, S., Hughes, A., Silveira, S., DeCarolis, J., Bazillian, M., Roehrl, A., 2011. OSeMOSYS: The Open Source Energy Modeling System. Energy Policy 39, 5850–5870. https://doi.org/10.1016/j.enpol.2011.06.033
IEA, 2023. SDG7: Data and Projections.
IEA, 2022. Africa Energy Outlook 2022.
Innovation landscape brief: Flexibility in conventional power plants, n.d.
IPCC, 2023. Climate Change 2022: Mitigation of Climate Change. Contribution of Working Group III to the Sixth Assessment Report of the Intergovernmental Panel on Climate Change. Cambridge University Press, Cambridge, UK and New York, NY, USA.
IRENA, 2024. The Energy Transition in Africa: Opportunities for International Collaboration with a Focus on the G7. International Renewable Energy Agency, Abu Dhabi.
IRENA, 2022. Renewable Energy Market Analysis: Africa and Its Regions. International Renewable Energy Agency and African Development Bank, Abu Dhabi and Abidjan.
Jewell, J., others, 2013. Energy Security under De-Carbonization Scenarios: An Assessment Framework and Evaluation under Different Technology and Policy Choices. Energy Policy 65, 743–760.

Kaufmann, A., D.&. Kraay, 2023. Worldwide Governance Indicators, 2023 Update.
Kenya Ends Oil Import Feud with Uganda, 2024. . East Afr.
Komendantova, N., others, 2012. Perception of Risks in Renewable Energy Projects: The Case of Concentrated Solar Power in North Africa. Energy Policy 40, 103–109.
Korkovelos, A., others, 2020. Supporting Electrification Policy in Fragile States: A Conflict-Adjusted Geospatial Least Cost Approach for Afghanistan. Sustainability 12, 777.
Kumar, A.R.S., Goyal, M.K., Ojha, C.S.P., Singh, R.D., Swamee, P.K., Nema, R.K., 2013. Application of ANN, Fuzzy Logic and Decision Tree Algorithms for the Development of Reservoir Operating Rules. Water Resour. Manag. 27, 911–925. https://doi.org/10.1007/s11269-012-0225-8
Macian-Sorribes, H., Pechlivanidis, I., Crochemore, L., Pulido-Velazquez, M., 2020. Fuzzy Postprocessing to Advance the Quality of Continental Seasonal Hydrological Forecasts for River Basin Management. J. Hydrometeorol. 21, 2375–2389. https://doi.org/10.1175/JHM-D-19-0266.1
Macian-Sorribes, H., Pulido-Velazquez, M., 2017. Integrating Historical Operating Decisions and Expert Criteria into a DSS for the Management of a Multi-reservoir System. J. Water Resour. Plan. Manag. 143, 04016069. https://doi.org/10.1061/(ASCE)WR.1943-5452.0000712
Mamdani, E.H., 1974. Application of fuzzy algorithms for control of simple dynamic plant. Proc. Inst. Electr. Eng. 121, 1585. https://doi.org/10.1049/piee.1974.0328
Marshall, M.G., Jaggers, K., 2015. Polity IV Project: Political Regime Characteristics and Transitions, 1800–2014.
O Dioha, M., others, 2023. Beyond Dollars and Cents: Why Socio-Political Factors Matter in Energy System Modeling. Environ. Res. Lett. 18, 121002.
Ofosu-Peasah, G., Ofosu Antwi, E., Blyth, W., 2021. Factors characterising energy security in West Africa: An integrative review of the literature. Renew. Sustain. Energy Rev. 148, 111259. https://doi.org/10.1016/j.rser.2021.111259
OSeMOSYS, n.d.
OSeMOSYS - TEMBA, n.d.
Otage, S., 2022. 12 High Voltage Power Lines Vandalised in Just a Month. Monitor.
Ou, Y., Binsted, M., Iyer, G., Patel, P., Wise, M., 2021. US state-level capacity expansion pathways with improved modeling of the power sector dynamics within a multisector model. Energy Strategy Rev. 38, 100739. https://doi.org/10.1016/j.esr.2021.100739
Panigrahi, D.P., Mujumdar, P.P., 2000. Reservoir operation modelling with fuzzy logic. Water Resour. Manag. 14, 89–109. https://doi.org/10.1023/A:1008170632582
Pappis, I., Howells, M., Sridharan, V., Usher, W., Shivakumar, A., Gardumi, F., Ramos, E., 2019. Energy projections for African countries. Publications Office of the European Union, LU.
Patankar, N., others, 2019. Building Conflict Uncertainty into Electricity Planning: A South Sudan Case Study. Energy Sustain. Dev. 49, 53–64.
Pfenninger, S., Hawkes, A., Keirstead, J., 2014. Energy systems modeling for twenty-first century energy challenges. Renew. Sustain. Energy Rev. 33, 74–86. https://doi.org/10.1016/j.rser.2014.02.003
Pfenninger, S., Staffell, I., 2016. Long-term patterns of European PV output using 30 years of validated hourly reanalysis and satellite data. Energy 114, 1251–1265. https://doi.org/10.1016/j.energy.2016.08.060
Riahi, K., Van Vuuren, D.P., Kriegler, E., Edmonds, J., O'Neill, B.C., Fujimori, S., Bauer, N., Calvin, K., Dellink, R., Fricko, O., Lutz, W., Popp, A., Cuaresma, J.C., Kc, S.,

Leimbach, M., Jiang, L., Kram, T., Rao, S., Emmerling, J., Ebi, K., Hasegawa, T., Havlik, P., Humpenöder, F., Da Silva, L.A., Smith, S., Stehfest, E., Bosetti, V., Eom, J., Gernaat, D., Masui, T., Rogelj, J., Strefler, J., Drouet, L., Krey, V., Luderer, G., Harmsen, M., Takahashi, K., Baumstark, L., Doelman, J.C., Kainuma, M., Klimont, Z., Marangoni, G., Lotze-Campen, H., Obersteiner, M., Tabeau, A., Tavoni, M., 2017. The Shared Socioeconomic Pathways and their energy, land use, and greenhouse gas emissions implications: An overview. Glob. Environ. Change 42, 153–168. https://doi.org/10.1016/j.gloenvcha.2016.05.009

Rukanga, B., 2023. How Kenya stands to lose from Uganda oil row. BBC News.

Russell, S.O., Campbell, P.F., 1996. Reservoir Operating Rules with Fuzzy Programming. J. Water Resour. Plan. Manag. 122, 165–170. https://doi.org/10.1061/(ASCE)0733-9496(1996)122:3(165)

Shrestha, B.P., Duckstein, L., Stakhiv, E.Z., 1996. Fuzzy Rule-Based Modeling of Reservoir Operation. J. Water Resour. Plan. Manag. 122, 262–269. https://doi.org/10.1061/(ASCE)0733-9496(1996)122:4(262)

Spalding-Fecher, R., Joyce, B., Winkler, H., 2017. Climate change and hydropower in the Southern African Power Pool and Zambezi River Basin: System-wide impacts and policy implications. Energy Policy 103, 84–97. https://doi.org/10.1016/j.enpol.2016.12.009

Spyrou, E., others, 2019. Planning power systems in fragile and conflict-affected states. Nat. Energy 4, 300–310. https://doi.org/10.1038/s41560-019-0346-x

Steduto, P., Hsiao, T.C., Fereres, E., Raes, D., 2012. FAO Irrigation and Drainage Paper 66: crop yield response to water.

Sterl, S., Devillers, A., Chawanda, C.J., Van Griensven, A., Thiery, W., Russo, D., 2022. A spatiotemporal atlas of hydropower in Africa for energy modelling purposes. Open Res. Eur. 1, 29. https://doi.org/10.12688/openreseurope.13392.3

Stevanato, N., Rocco, M.V., Giuliani, M., Castelletti, A., Colombo, E., 2021. Advancing the representation of reservoir hydropower in energy systems modelling: The case of Zambesi River Basin. PLOS ONE 16, e0259876. https://doi.org/10.1371/journal.pone.0259876

SWAT+, n.d.

Taliotis, C., Shivakumar, A., Ramos, E., Howells, M., Mentis, D., Sridharan, V., Broad, O., Mofor, L., 2016. An indicative analysis of investment opportunities in the African electricity supply sector — Using TEMBA (The Electricity Model Base for Africa). Energy Sustain. Dev. 31, 50–66. https://doi.org/10.1016/j.esd.2015.12.001

Tidball, R., Bluestein, J., Rodriguez, N., Knoke, S., International, I., Macknick, J., 2010. Cost and Performance Assumptions for Modeling Electricity Generation Technologies. Renew. Energy.

Trotter, P.A., others, 2018. Solar Energy's Potential to Mitigate Political Risks: The Case of an Optimised Africa-Wide Network. Energy Policy 117, 108–126.

UN, n.d. Goal 7: Ensure access to affordable, reliable, sustainable and modern energy for all.

Van Beek, L.P.H., Wada, Y., Bierkens, M.F.P., 2011. Global monthly water stress: 1. Water balance and water availability. Water Resour. Res. 47, 2010WR009791. https://doi.org/10.1029/2010WR009791

Van Vuuren, D.P., others, 2011. The Representative Concentration Pathways: An Overview. Clim. Change 109, 5.

Wada, Y., Bierkens, M.F.P., De Roo, A., Dirmeyer, P.A., Famiglietti, J.S., Hanasaki, N., Konar, M., Liu, J., Müller Schmied, H., Oki, T., Pokhrel, Y., Sivapalan, M., Troy, T.J., Van

Dijk, A.I.J.M., Van Emmerik, T., Van Huijgevoort, M.H.J., Van Lanen, H.A.J., Vörösmarty, C.J., Wanders, N., Wheater, H., 2017. Human–water interface in hydrological modelling: current status and future directions. Hydrol. Earth Syst. Sci. 21, 4169–4193. https://doi.org/10.5194/hess-21-4169-2017

Wasti, A., others, 2022. Climate Change and the Hydropower Sector: A Global Review. WIREs Clim. Change 13, e757.

Zeng, Y., others, 2011. A Review on Optimisation Modeling of Energy Systems Planning and GHG Emission Mitigation under Uncertainty. Energies 4, 1624–1656.

Zerriffi, H., Dowlatabadi, H., Strachan, N., 2002. Electricity and Conflict: Advantages of a Distributed System. Electr. J. 15, 55–65. https://doi.org/10.1016/S1040-6190(01)00262-7